Consulting services for mathematical modeling of fluid flow, heat transfer, and/or chemical reaction processes.

CHAM

ANALYSIS OF PHYSICAL-CHEMICAL PROCESSES
GOVERNING SSME INTERNAL FLUID FLOWS

PROGRESS REPORT FOR MAY 1985

by

A.K. Singhal, S.F.Owens, T. Mukerjee,
C. Prakash, A.J. Przekwas and M. Kannapel

June 1985   4045/22

Prepared for:

CONTENTS

TABLE OF CONTENTS

APPENDIX A

    Interim Report on Thermofluid Analysis of the SSME Fuel
    Side Preburner

APPENDIX B

    Interim Report on External Tank Slump Problem

APPENDIX C

    Interim Report on Global Modeling of SSME

PREFACE

This progress report summarizes the work performed during May 1985, and discusses the work to be performed during June 1985. It also indicates the estimates of project progress in terms of percentage completion of each task and of the total work scheduled for the first two years of the contract.

Technical discussions with NASA MSFC ED42 and EL24 personnel are gratefully acknowledged.

INTRODUCTION

In order to aid the development of current and future (advanced) SSME type engines, it is necessary to improve the understanding of basic issues concerned with physical-chemical processes of SSME internal flows. Towards this goal, the specific objectives of the project are

1. to supply the general-purpose CFD code PHOENICS and the associated interactive graphics package - GRAFFIC;

2. to demonstrate code usage on SSME-related problems to NASA MSFC personnel;

3. to perform computations and analyses of problems relevant to current and future SSME's; and

4. to participate in the development of new physical models of various processes present in SSME components.

The total project duration is three years. This is the progress report for the month of May 1985 (i.e. first month of the second year of performance).

WORK PERFORMED DURING MAY 1985

During the month of May 1985, attention was focused on Tasks 2, 3, 4 and 5. Accomplishments under each of these tasks are described below.

Task 2: Interface Codes with MSFC Facility and Personnel

Under this task necessary user support was provided to ED42 personnel for the use of (a) satellites and ground stations of PHOENICS transferred in December 1984 and earlier; and (b) the GRAFFIC code. In the current month CHAM's AUTOPLOT program was installed on NASA's PE 3252 computer. This program is now available from PHOENICS User's Group account number 24 and is called AUTOPLOT.TSK. The program can be executed by entering AUTOPLOT/G from any interactive graphics terminal. The relevant documentation on the use of AUTOPLOT was provided.

Task 3: Flow Physics Applications

A technical paper on Hot Gas Manifold Flow Analysis was prepared and submitted to NASA project manager for comments. Additional data for thermal analysis of Hot Gas Manifold (HGM) of SSME Fuel Preburner have been received. They consist of:

a) HGM inlet or High Pressure Fuel Turbine (HPFT) discharage <u>gas temperature</u> measured at two locations;

b) HGM (with three transfer tubes) <u>gas temperatures</u> measured at the middle tube exit and the right tube (viewed from HGM towards LOX posts) exit;

c) Fuel Preburner Bowl <u>surface temperatures</u> at 15 locations; and

d) Main Injector Assembly (MIA) LOX-post-shield <u>surface temperatures</u> at one location.

Of the above only a) and b) are concerned with HGM but they are gas temperature measurements, not wall surface temperatures which are required for the thermal analysis of HGM. In view of this a method needs to be explored for starting the HGM analysis with the available thermal data. .

Task 4: Multi-Fluid Model/Fuel-Side Preburners

Analysis of combustion and mixing in the SSME fuelside preburner using the two-fluid approach has been extended further by incorporating Magnussen's eddy-break-up model to compute the rate of combustion within the gaseous phase (Phase 1). Results are compared with those obtained last month (CHAM 4045/17) using the instantaneous reaction model. The interphase mass transfer is found to be slightly less for the eddy break-up model. Within Phase 1, the eddy break-up model predicts incomplete combustion and finite mass fraction of unburnt oxygen gas all the way up to the burner exit; in contrast, the instantaneous reaction model predicts complete combustion and zero oxygen

2

concentration everywhere within Phase 1. Due to incomplete combustion, the eddy break-up model predicts lower temperatures compared to the instantaneous reaction model. The possibility of unburnt liquid oxygen and high dome temperatures is predicted by the models. Details of the study and plans for further work are included in Appendix A, Part 1.

The only unknown parameter in the model is the diameter of the oxygen droplets at the preburner inlet. A literature search has been initiated to identify material that can provide useful guidance in this regard. Some reliable sources of information have already been found and an estimate of d_0 is presented in Part 2 of Appendix A.

Task 4a: External Tank Slump Problem

Last month the results of a sloshing problem were reported. The liquid was initially tilted with respect to gravity and was allowed to move with no excitation other than gravity. That problem demonstrated that the donor-acceptor method in PHOENICS is capable of yielding plausible results for two phase flows with sharp interphase. This month, an effort has been made to incorporate more of the physical properties of the External Tank into the model. The model is now a cylindrical tank, with the same global dimensions as that of the External Tank. Proper compressibility, viscosities, and other properties were included in the model. The test problems this month are also closer to the real case. The motion within the tank was caused by a deflection of the tank wall at various locations, with the effects of a baffle and the position of the deflection being examined and reported in Appendix C. The deflection was simply a ramp function approximation of the first quarter of a cycle of a sawtooth wave. So, these runs were obtained by pushing the wall in but not letting it come back out.

Next month several steps are planned: calculations with a more refined grid, introduction of sinusoidal time variation of the wall deflection, deflecting the wall at more than one point, and preparing to include the correct External Tank shape and the correct surface level.

Task 5: SSME Global Flow Model

As a part of the global model, a 3-D simulation of the Main Injector Assembly (MIA) was reported last month wherein non-uniform velocity distributions at Fuel Preburner End (FPE) and at Oxygen Preburner End (OXPE) were used. At the FPE the velocity distribution was provided through a "processor-program" that processed the Hot Gas Manifold (HGM) exit velocity distribution in BFC system to the orthogonal polar grid system used in MIA while assuring simultaneously the required mass inflow. In this report, the linearly varying velocity distribution at OXPE entry was replaced by a realistic non-uniform velocity distribution using the processor-program and test runs were made with and without shields on outer row of LOX posts. Details of the above are given in Appendix C.

Development and try out of a two-way coupling program is continuing for a simplified geometry where fluid from a 2-D (cartesian grid) duct enters into a straight and enlarged rectangular duct and flows out further downstream. The computed results will be compared with the case when both geometries are covered by a single grid and solved for flow and pressure distribution. These findings will be reported next month.

WORK PLANNED FOR JUNE 1985

During the month of June, work will continue on Tasks 2, 3, 4 and 5, as explained in the previous subsections.

CURRENT PROBLEMS

No problems are envisaged which may impede performance of this project.

PROGRESS SUMMARY

A taskwise progress status is shown in the table below. Estimated total percentage completion through May is 64% of the first two year's scope of work.

NO.	TASK DESCRIPTION	% COMPLETION OF FIRST TWO YEARS EFFORT, AS ON MAY 31, 1985
1.	Provide PHOENICS and GRAFFIC codes	100
2	Interface codes with MSFC Facility and Personnel	90
3	Flow Physics Applications	80
4	Multi-Fluid (Phase) Model	60
5	SSME Global Flow Model	60
6	Reports	Monthly Progress Reports

APPENDIX A

Interim Report on Thermofluid
Analysis of the SSME Fuel Side Preburner

by

C. Prakash and A.K. Singhal

THERMOFLUID ANALYSIS OF THE SSME FUELSIDE
PREBURNER USING A TWO-FLUID MODEL

1. PROBLEM DESCRIPTION

During last month (CHAM 4045/17), the two fluid model, with local expressions for the exchange coefficients C_M and C_F, was applied to analyse combustion in the SSME preburner. Within the gaseous phase, called Phase 1, combustion was assumed to be instantaneous. In reality, the assumption of instantaneous reaction may not be quite valid, and hence, these computations have been repeated using the Magnussen's eddy break-up model to compute the reaction rate. Details of the eddy break-up model may be found in CHAM 4045/13. The geometrical details and grid layout are shown in Figure A1; for details, see CHAM 4045/5.

2. RESULTS

The results of the present study are summarized in Figures A2, A3 and A4, which correspond to the inlet oxygen droplet diameter d_0 of 254, 127 and 25.4 µm respectively. In each figure, the left panel describes results obtained by the eddy break-up model, and the right panel corresponds to the instantaneous reaction model.

Here r_2 represents the volume fraction of liquid oxygen (Phase 2), T is the temperature of the gas phase (Phase 1), m_{ox} is the mass fraction of unburnt oxygen gas within Phase 1, and C_M and C_F are the mass and momentum exchange coefficients. The following conclusions may be drawn.

(i)   Due to a finite reaction rate equation in the eddy break-up model, combustion is weak as compared to the instantaneous reaction model. In fact, the eddy break-up model predicts finite amount of unburnt oxygen gas (m_{ox}) within Phase 1 all the way up to the burner exit. In contrast, for the instantaneous reaction model, m_{ox} was found to be zero everywhere implying complete combustion.

A1

(ii)   Due to the weaker combustion implied by the eddy break-up model, the temperature of the gas phase is generally lower as compared with that predicted by the instantaneous reaction model. The exception is the case of d_0 = 25.4 μm where some local regions of higher temperature are predicted by the eddy break-up model.

(iii)   Experimental tests have revealed the occurance of high temperatures and unburnt liquid oxygen over the turbine dome. According to the present computations, higher dome temperatures (compared with the average exit temperature) are predicted by the eddy break-up model for all the d_0 values considered, and by the instantaneous reaction model for d_0 = 254 μm. Unburnt liquid oxygen over the dome is predicted by either model for d_0 = 254 μm. As will be discussed shortly, plans for immediate future work include an effort aimed at making a good estimate of d_0; nevertheless, it is quite encouraging to note from the present computations that the model being pursued does have the potential of predicting the high temperatures and unburnt oxygen over the dome top.

(iv)   Smaller value of r_2 at a point implies that a greater amount of mass transfer has taken place from Phase 2 to Phase 1. Hence it may be concluded from the figures that the eddy break-up model implies a slightly smaller interphase mass transfer as compared to the instantaneous reaction model. This can be understood by examining the interphase mass transfer equation which reads[+],

$$\left\{ \begin{matrix} \text{Interphase mass transfer} \\ \text{per unit volume per unit time} \end{matrix} \right\} = \frac{12}{d^2} \, r_2 \, \frac{\lambda}{C_p} \, \ell m \, (1 + B_{ev}) \, (1 + .244 \, \sqrt{Re})$$

where

$$B_{ev} = \frac{C_p \, (T_g - T_\ell)}{h_{fg}}$$

[+] the different terms are described in CHAM 4045/17.

A2

The influence of the combustion model on the interphase mass transfer is primarily through the evaporative driving potential $(T_g - T_\ell)$ where T_g and T_ℓ represent the temperature of the gas (Phase 1) and the liquid oxygen (Phase 2). Since, as already discussed, T_g is generally small for the eddy break-up model, this driving potential is also small, and hence the mass exchange is less.

3. PLANS FOR FURTHER WORK

Some useful sources of information needed for obtaining a reliable estimate of d_0 have already been identified (see Part 2). This search has to be continued further, and some of the two-fluid calculations will be repeated with such d_0 values.

Part 2 Estimate of d_0

The report:[+]

NASA SP-194 "Liquid Propellant Rocket Combustion Instability", Edited by D.T. Harrje and F.H. Reardon, 1972.

has been identified as a useful source of information. The mechanisms of atomization, alongwith the expressions for d_0 and the jet break-up length, are described at length in section 2.2.3 (pages 49-55). Of a number of expressions listed, the empirical correlation of Hirsch and Rice:

$$d_0 \sim \frac{V_j}{\Delta V} \left(\frac{d_j^3}{y}\right)^{1/2}$$

is recommended for concentric tube injectors like the ones employed in the SSME preburner. In this expression:

V_j = Velocity of liquid jet

(ΔV) = Velocity difference between the liquid jet and the surrounding gas in the annulus

d_j = diameter of liquid jet

y = width of annualr gas passage

In the case of the preburner,

V_j = 27.96 m/s

ΔV = (306.36 - 27.96) = 278.4 m/s

d_j = .002261 m

y = .0008227 m.

Substituting in the d_0 expression we get

$d_0 \sim \underline{376 \ \mu m}$ ($\approx \frac{1}{6}$ th of jet diameter)

This value of d_0 appears to be high. The original report of Hirsch and Rice is now to be studied for further classifications.
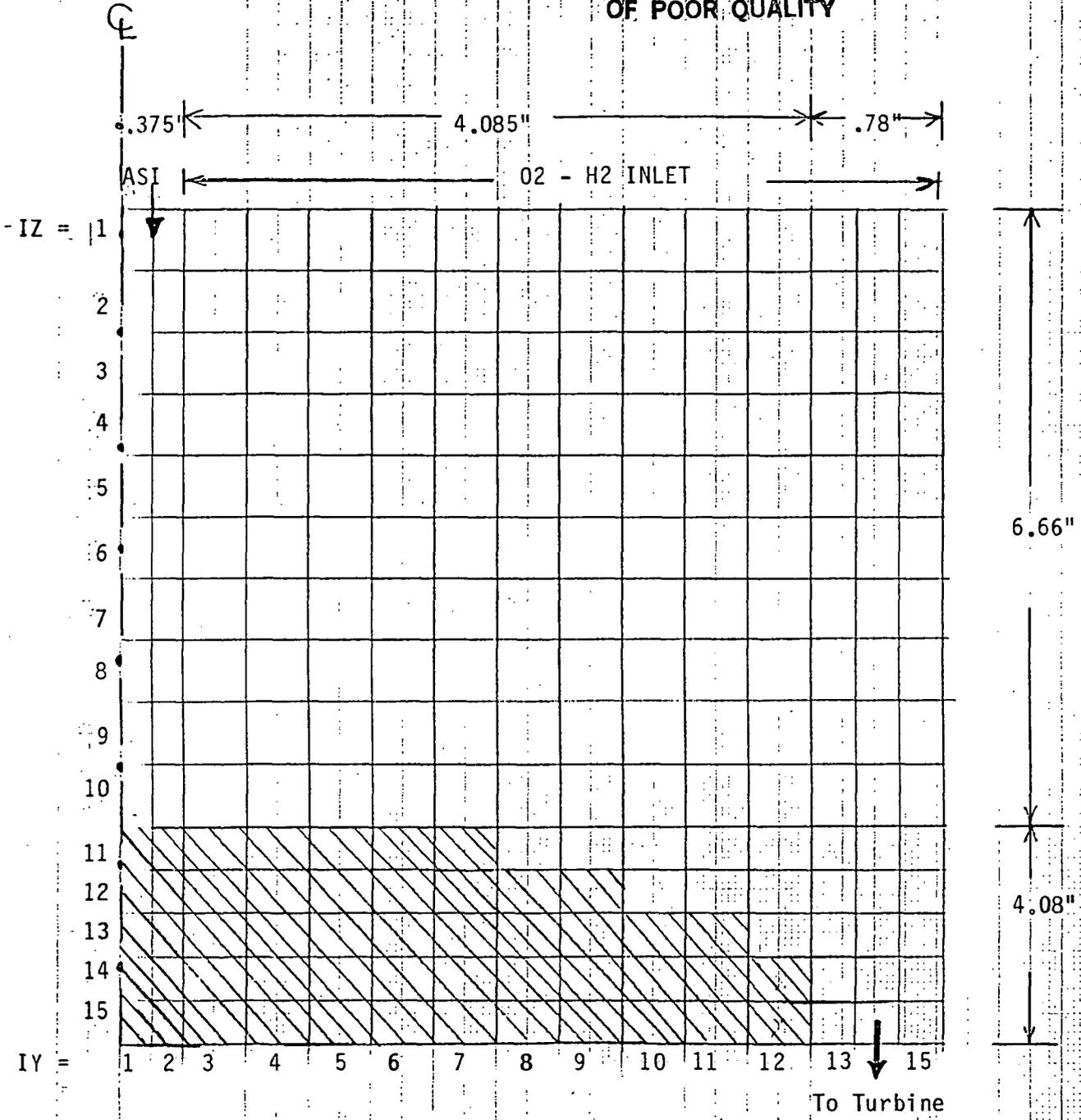
Figure A1. Grid Layout for the Preburner
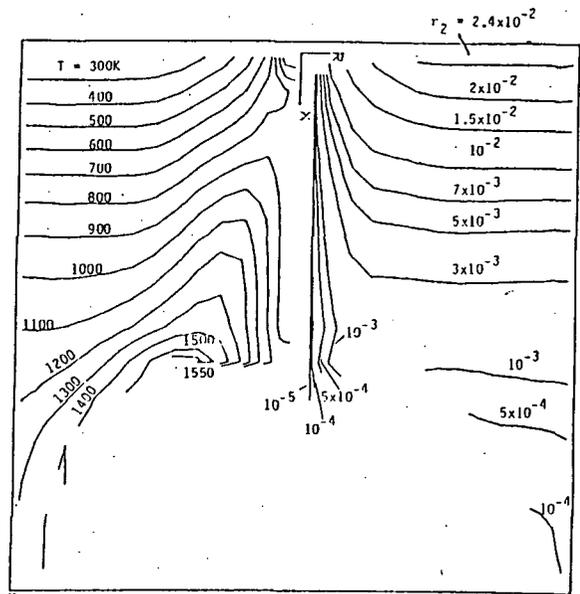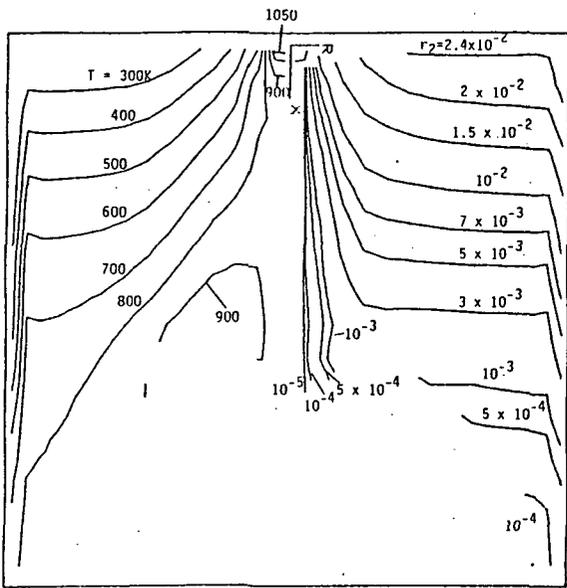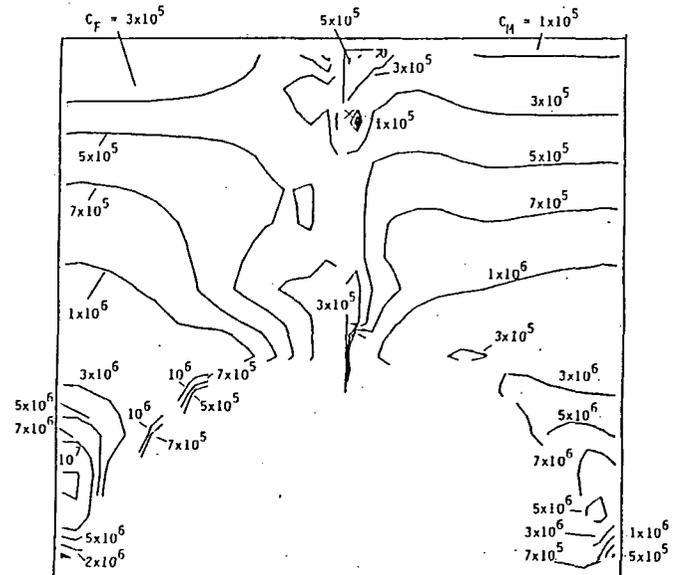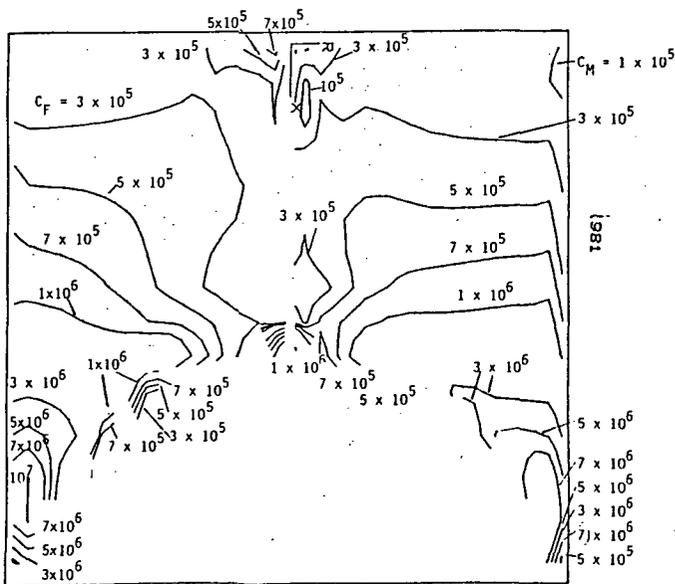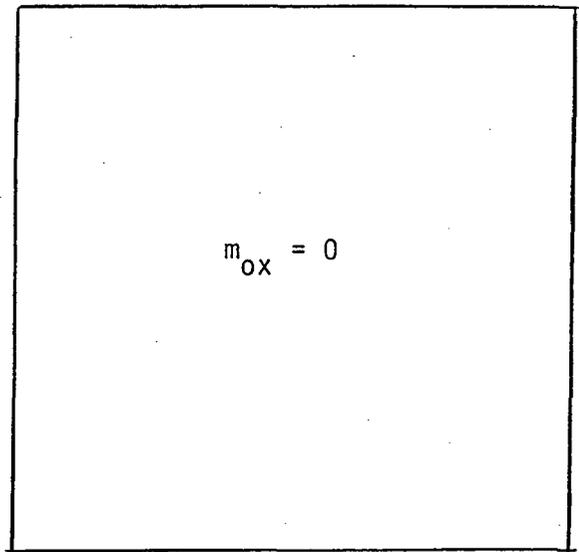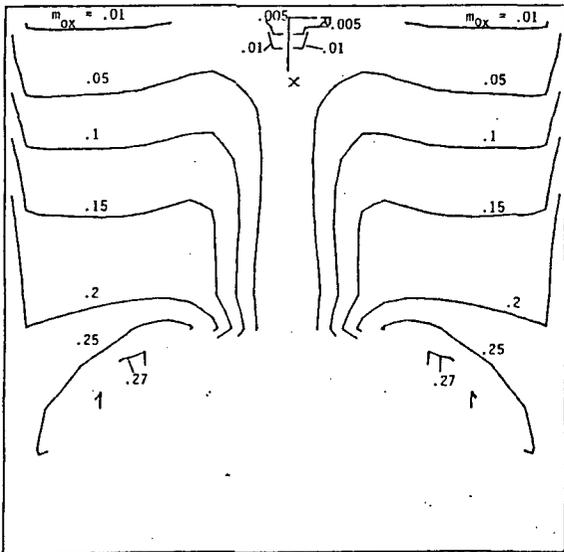
EDDY BREAKUP MODEL

INSTANTANEOUS REACTION MODEL

Figure A2. Results for $d_o = 254$ μm
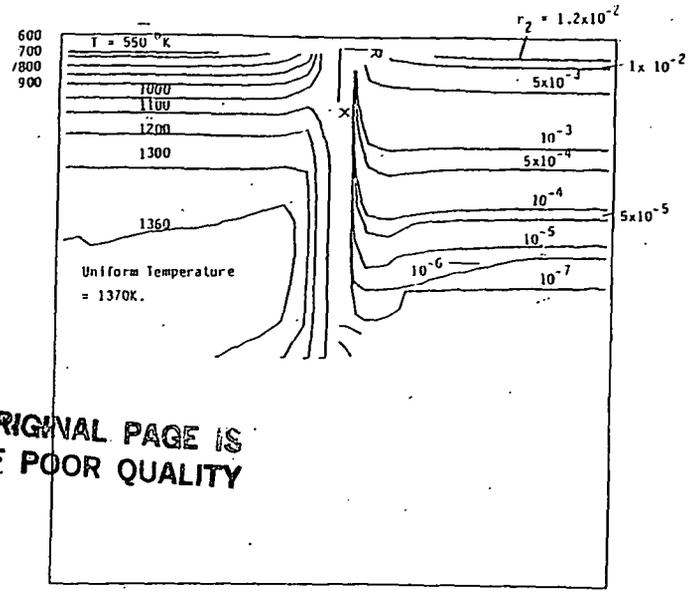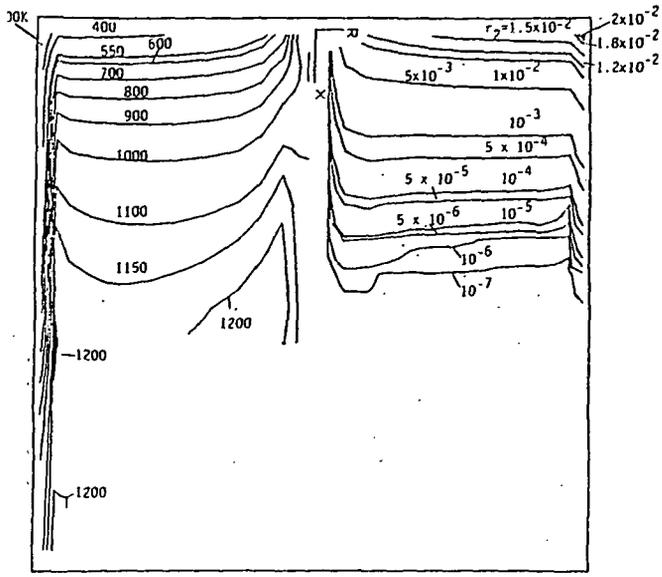
A6
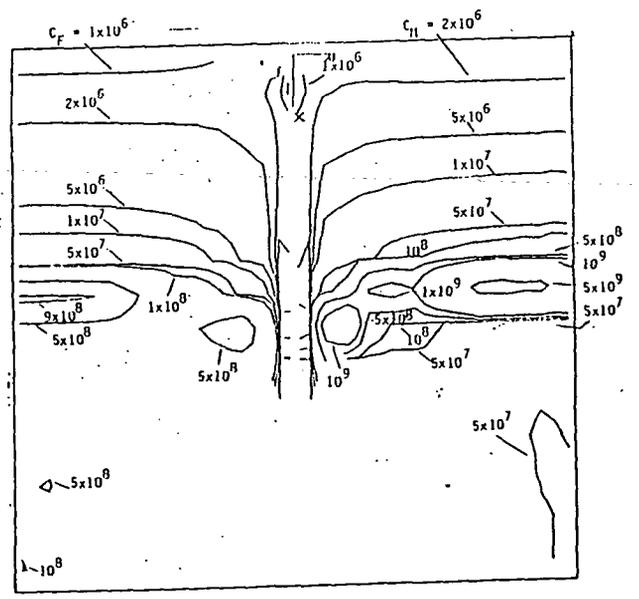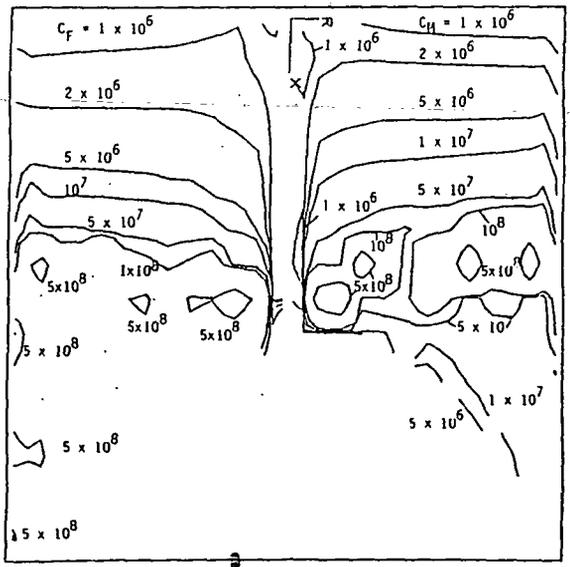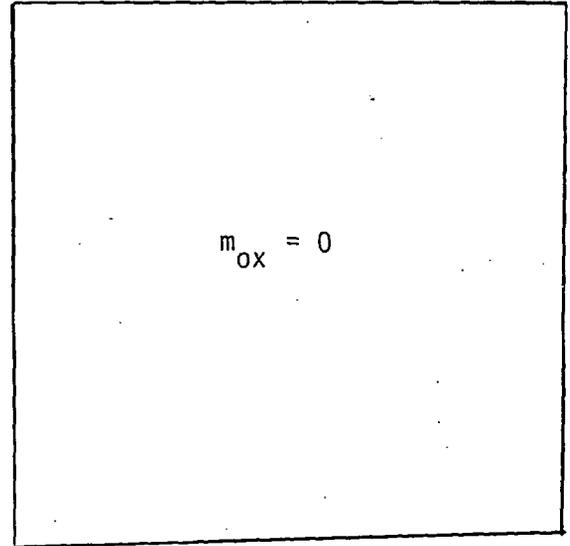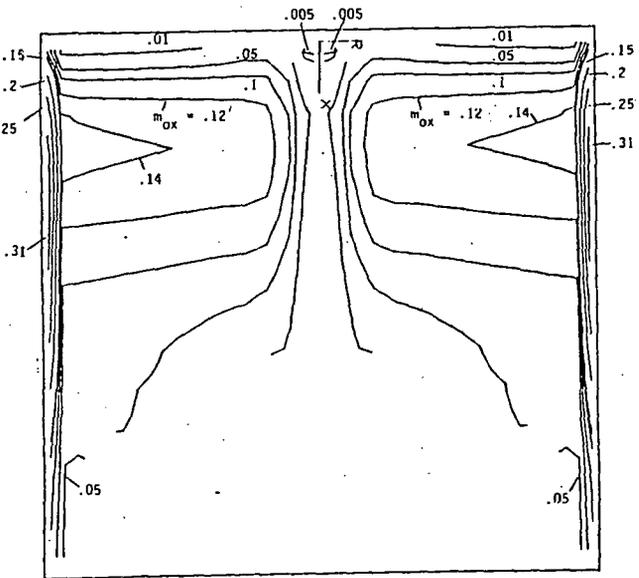
EDDY BREAKUP MODEL

INSTANTANEOUS REACTION MODEL

Figure A3. Results for d_o = 127 μm

A7
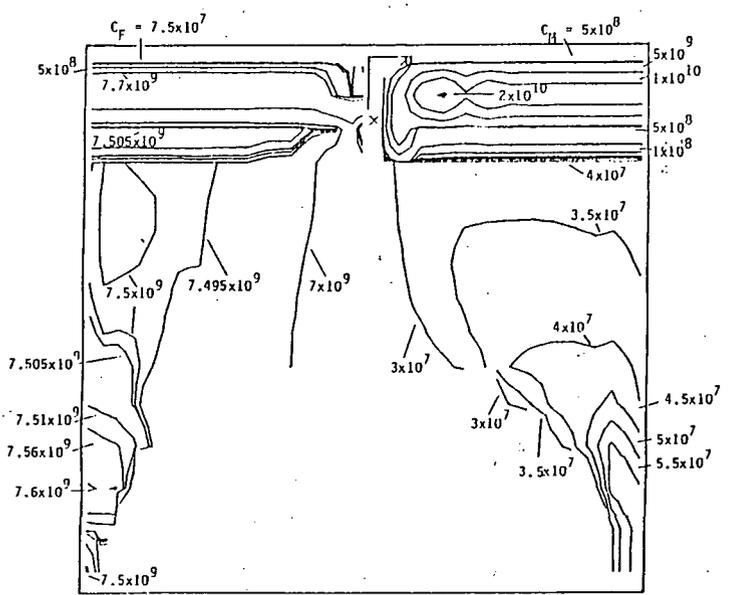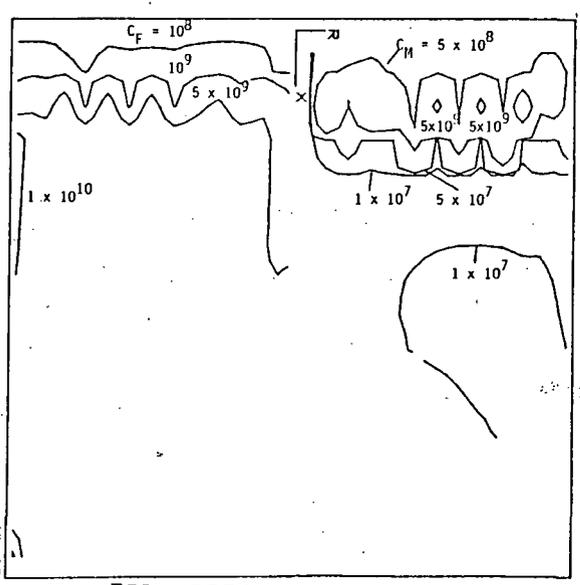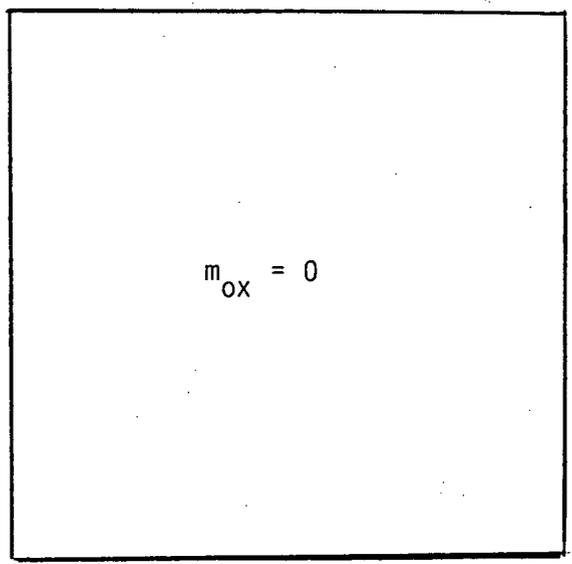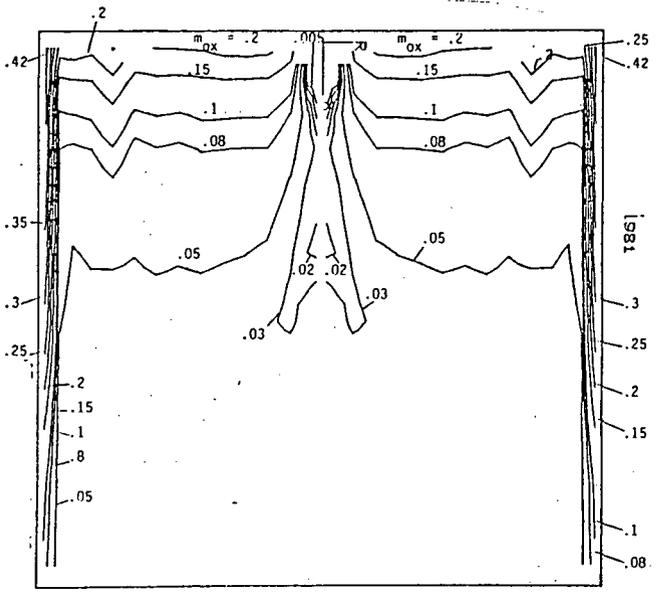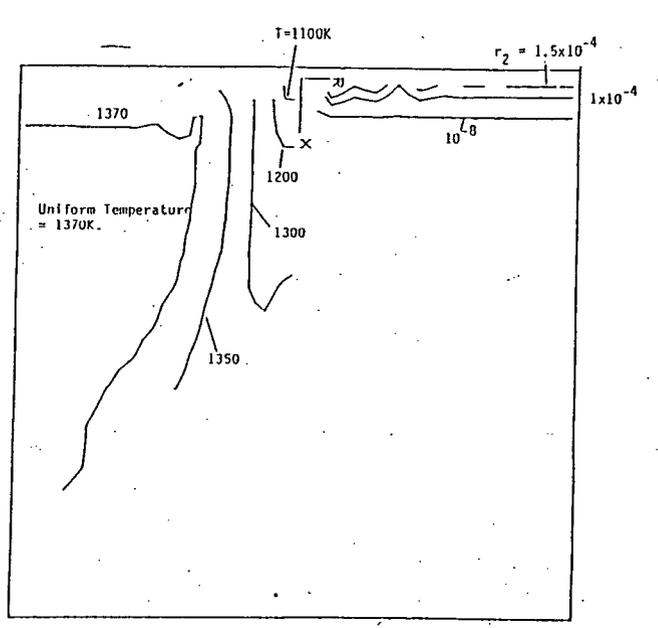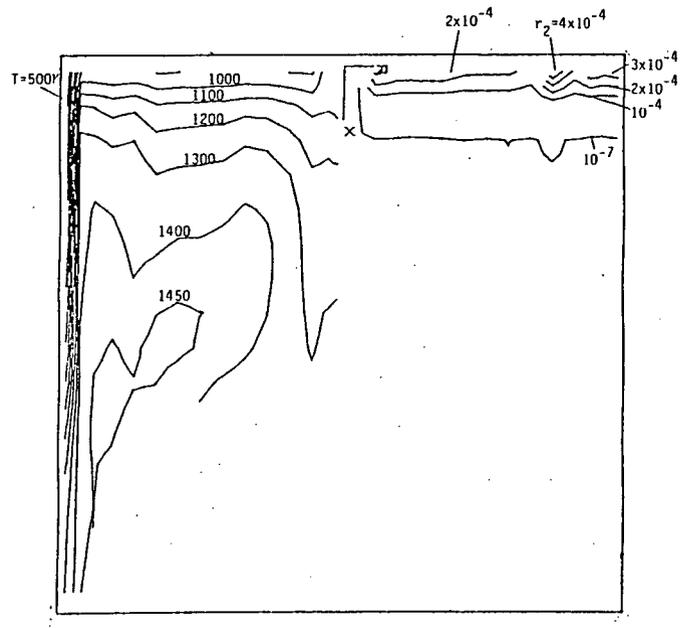
EDDY BREAKUP MODEL

INSTANTANEOUS REACTION MODEL

Figure A4. Results for d_0 = 25.4 μm

A8

APPENDIX B

Interim Report on
External Tank Slump Problem

by
M.D. Kannapel, A.J. Przekwas and A.K. Singhal

ABSTRACT

Since last month's sloshing problem the model has been refined to include a cylindrical tank (instead of rectangular), proper compressibility terms, reference densities and viscosities. Most of the experimental runs have been made by inducing motion into the system by deflecting the tank wall at various locations. The effect of a baffle and of the deflection location has been examined with selected results being reported. The anticipated next steps in the project are also outlined.

INTRODUCTION

Last months sloshing problem was aimed at verifying that PHOENICS is capable of using the Donor Acceptor method to predict fluid flow with an interphase. This month, an effort has been made to create a working model that more closely approximates the actual conditions of the External Tank. Compressibility effects of both liquid oxygen (LOX) and gaseous oxygen (GOX) were examined with trial runs revealing that only the GOX need be considered compressible. Correct reference densities and viscosities were found by assuming the saturation temperature at a pressure of 20 psia.

Here, results of, calculations are reported on a cylindrical tank having the same global dimensions as the External Tank (Figure B1). The motion of the LOX was induced by deflections of the cylinder wall at various locations with the effects on the surface being examined closely.

COMPUTATIONAL DETAILS

The grid employed in all calculations is very similar to the grid used in last months sloshing calculations, the only difference being the use of cylindrical coordinates instead of rectangular coordinates (see Figure B1). As mentioned above, for these calculations, the motion within the cylinder was caused by a deflection of the cylinder wall. This deflection follows the first quarter of a sawtooth wave with a frequency of four Hz, with no further deflection occuring after the first quarter cycle. Figure B2 shows how the wave was approximated with a ramp function. The time step for each run was 0.00625 sec until the tank wall was completely deflected and 0.02 sec for the remaining time. Checkout runs were performed to ensure that the mass of each phase remained constant. The effect of interphase friction was also examined with the results showing little dependence on this parameter. Several test runs were made to determine whether a momentum source is necessary where the deflection occurs. The momentum source, in the radial direction, was found to have noticeable effects on results and was therefore included in all calculations.

PRESENTATION AND DISCUSSION OF RESULTS

Although several cases have been examined, this report presents selected results from two test cases:

Case 1:   Deflection of part of one cell near the bottom of the tank with a comparison of the surface movement with and without a baffle.

Case 2:   Comparison of surface movement with a deflection near the liquid surface and with a deflection near the bottom.

The position of the two deflection points, the baffle, and the liquid surface are shown in Figure B1. For each case two types of results are provided: velocity vectors with the surface location shown in the proper scale (Figure B3 and B5), and an enlarged view of the surface allowing the shape and size of the surface displacement to be observed (Figures B4 and B6). In all runs the surface displacements are so small that the surface never crosses over a cell boundary. Therefore, the surface shape can be examined by looking at how the surface moves in one cell. In the enlarged surface plots the Y-axis is the volume fraction (RZ) of the cell where the surface is located. When RZ=0, the cell contains all gas; when RZ=1, the cell contains all liquid. The Y-axis scale is also given in meters and inches. The x-axis is the radial distance across the cylinder (0 meters = centerline, 4 meters = wall).

Results of Case 1 show that, for large deflections (1/12 of the tank radius), much larger surface disturbances occur with the baffle inserted than without it, although in both runs the displacement is very small. The shape of the surface is also different; with the baffle, it rises in the center first. Without the baffle, it rises near the wall first. Results of Case 2 show that a wall deflection near the surface has a much larger effect on the surface shape than a similar deflection near the bottom of the tank.

CONCLUSIONS AND RECOMMENDATIONS

Although the results of the parametric studies can-not be directly generalized to the External Tank conditions, (i.e. different tank shape, surface level,

deflected volume and position, baffle placement and size) they still show that our model is capable of responding plausibly to these input parameters.

The next steps planned to be undertaken for this project include the following:

- calculations with a more refined grid;

- introduction of sinusoidal time variation of the wall deflections;

- deflecting the wall at more than one position at a time; and

- preparation of code modifications to accommodate the ET shape, correct surface level, and correct wall deflections as specified by NASA.

PROBLEM 2: WALL DEFLECTION IN AN ENCLOSED CYLINDRICAL TANK

- GEOMETRY AND COMPUTATIONAL GRID
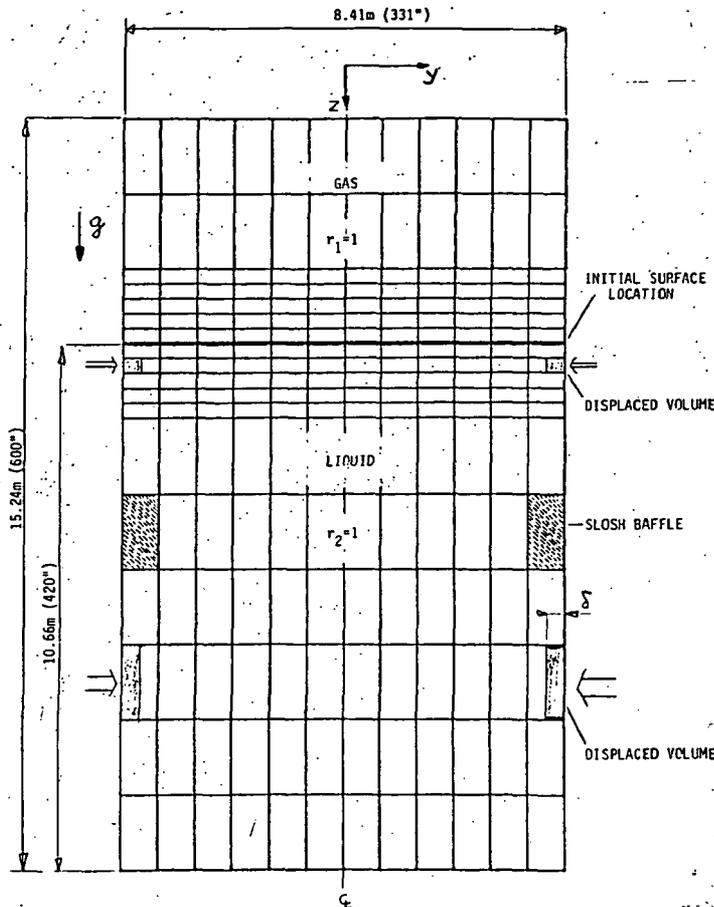
CYLINDRICAL POLAR
NZ * NY = 18 x 6
(108)
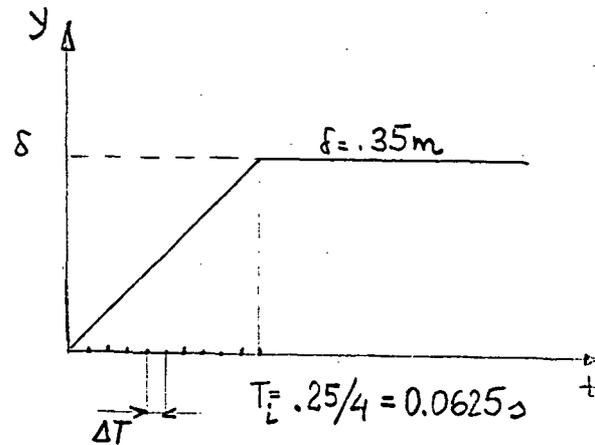
Figure B1

DISPLACEMENT TIME VARIATION

Figure B2

- FLUID PROPERTIES: TWO-PHASE FLOW WITH SHARP INTERFACE,

LOX: $168^\circ R$ (93K)

ρ_L = 70.24 lb/cuft (1125. kg/m^3)

μ_L = 12.10^5 lb/fts (18.10^{-5} kg/ms)

INCOMPRESSIBLE

GOX: SATURATION AT 20 psia

ρ_g = 0.37 lb/cuft (6.0 kg/m^3)

μ_g = 0.48 . 10^{-5} lb/fts (0.71 . 10^{-5} kg/ms)

a = 590 $\frac{ft}{s}$ (179.8 m/s) OR $\frac{\partial \rho}{\partial p}$ = 3.1 . 10^{-5} s/m

DEFLECTION NEAR BOTTOM
WITHOUT BAFFLE

DEFLECTION NEAR BOTTOM
WITH BAFFLE
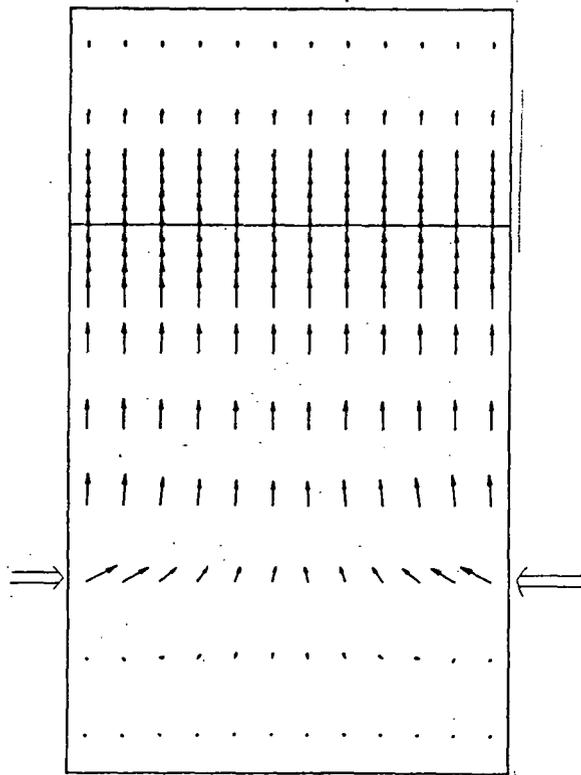
t = 0.0625
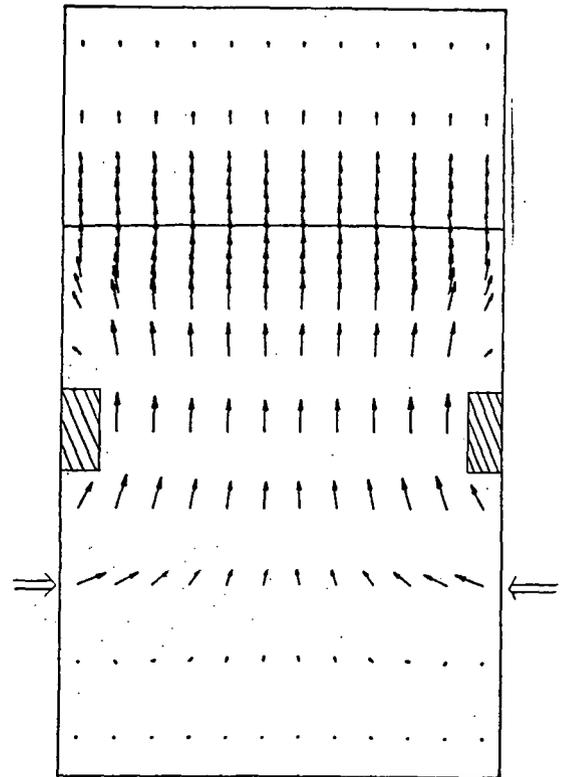
t = 0.0625
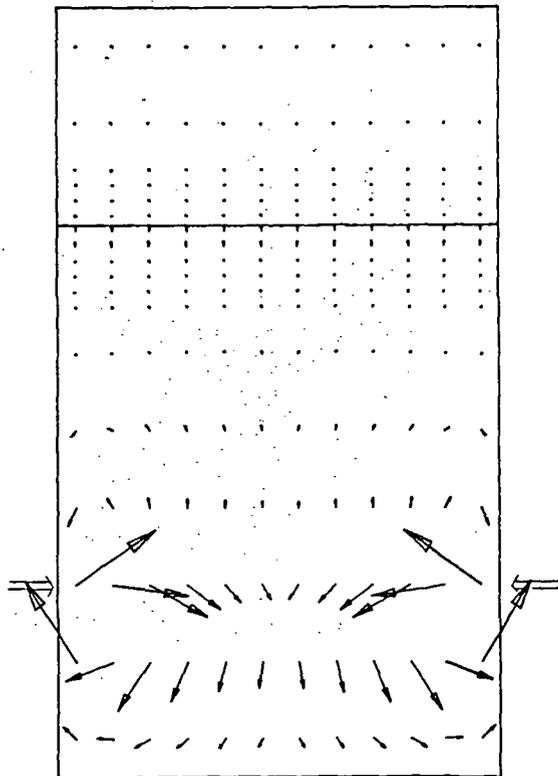
t = 0.4625
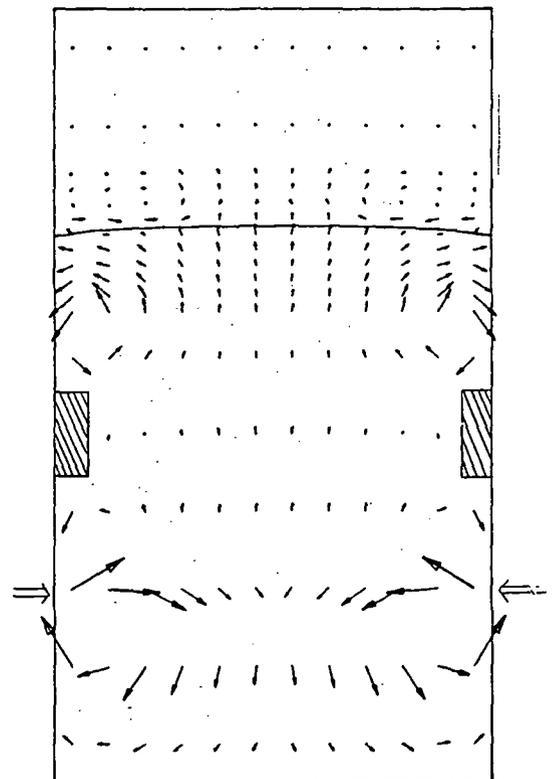
t = t = 0.4625

Figure B3:   Case 1 Velocity Vectors and Surface Positions

DEFLECTION NEAR BOTTOM WITHOUT BAFFLE

0.00427 m
(0.168 in)

R2

t = 0.6625

t = 0.4625

t = 0.2625

t = 0.0625   at t = 0, R2 = 0

0.772
0.770
0.768
0.766
0.764
0.762
0.760
0.758

0   1   2   3   4
CENTER   WALL
LINE   Y (METERS)

DEFLECTION NEAR BOTTOM WITH BAFFLE

R2

0.1829 in
(7.20 in)

1.0
0.8
0.6
0.4

at t = 0, R2 = 0

t = 0.8625
t = 0.0625
t = 0.6625
t = 0.2625
t = 0.4625

0   1   2   3   4   (157 inches)
CENTER   WALL
LINE   Y (METERS)
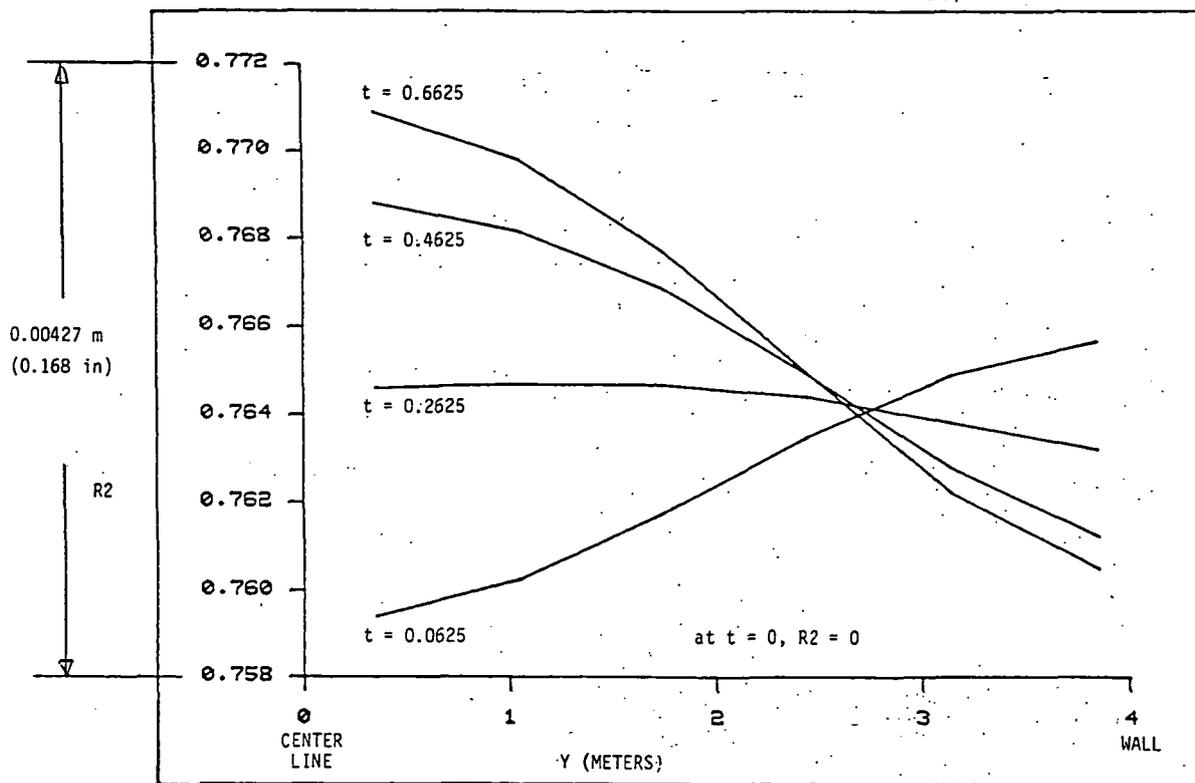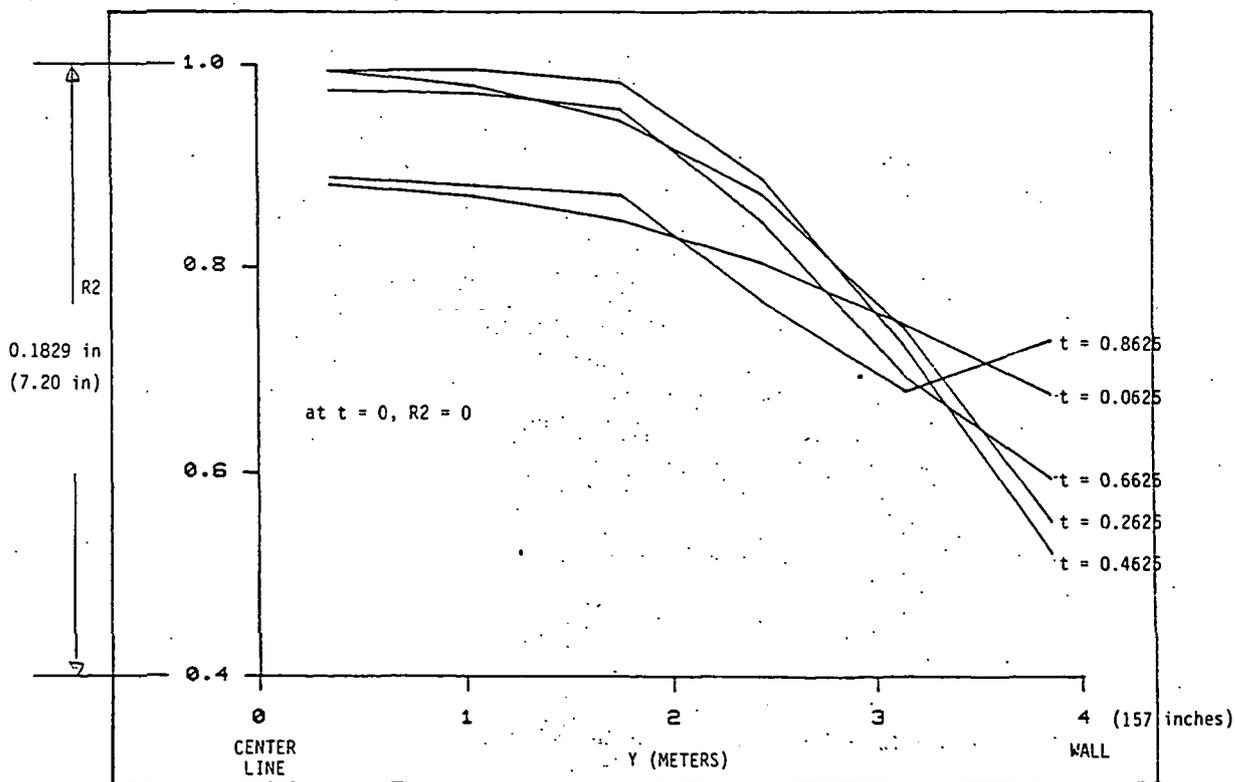
Figure B4: Case 1 Enlarged Surface Position

B7
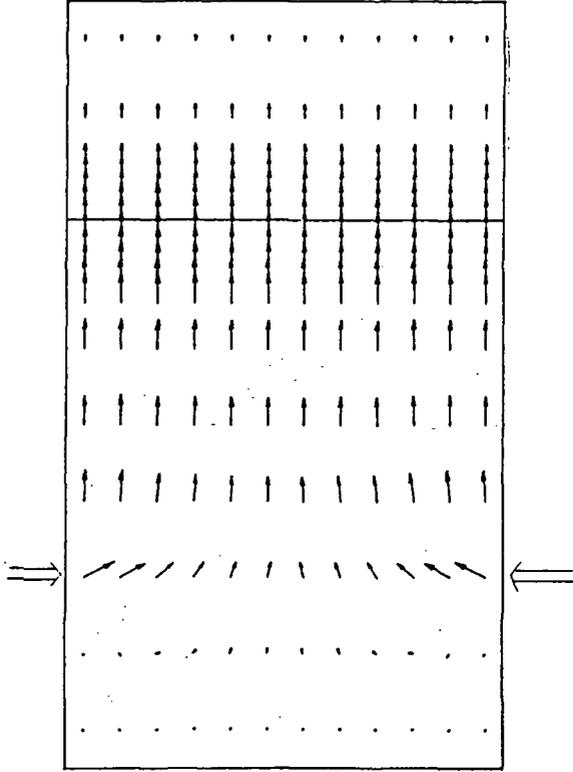
DEFLECTION NEAR
BOTTOM

DEFLECTION NEAR
TOP
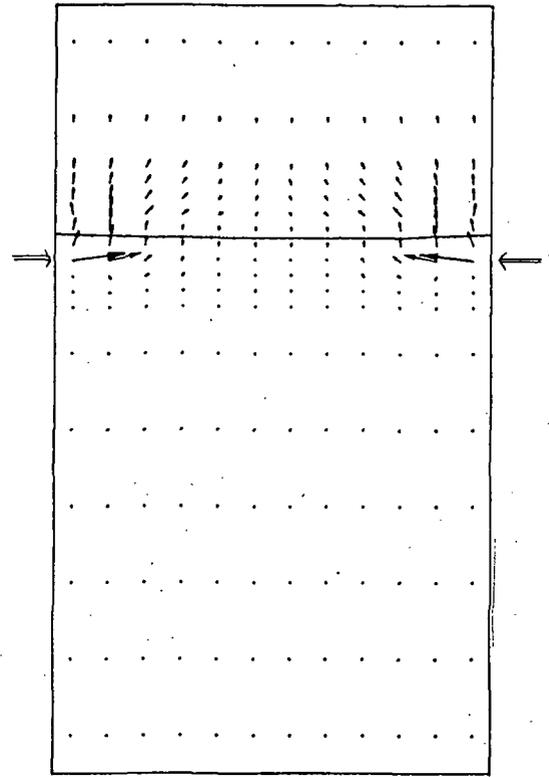
t = 0.0625

t = 0.0625
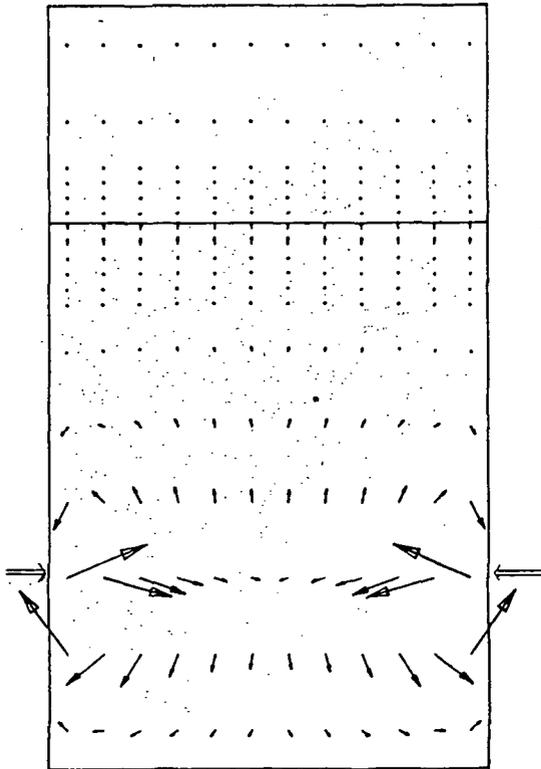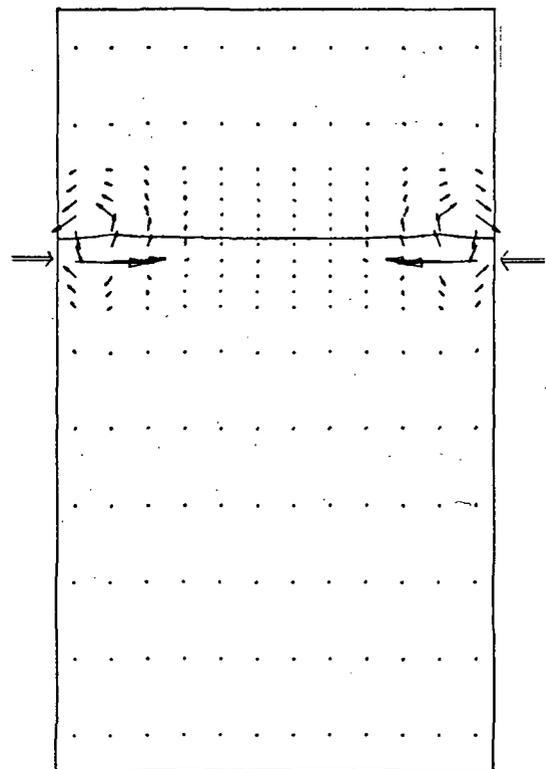
t = 0.1425

t = 0.1425

Figure B5: Case 2 Velocity Vectors and Surface Positions

DISPLACEMENT NEAR BOTTOM

t = 0.6625
t = 0.4625
t = 0.2625
t = 0.0625

at t = 0, R2 = 0

0.00427 m
(0.168 in)

R2

0.772
0.770
0.768
0.766
0.764
0.762
0.760
0.758

0   1   2   3   4
CENTER   WALL
LINE
Y (METERS)

DISPLACEMENT NEAR TOP

0.4
0.3
0.2
0.1
0.0

0.122 m
(4.80 in)

AT t = 0, R2 = 0

t = 0.2625
t = 0.2625
t = 0.4625

0   1   2   3   4 (157 in)
CENTER   WALL
LINE
Y (METERS)
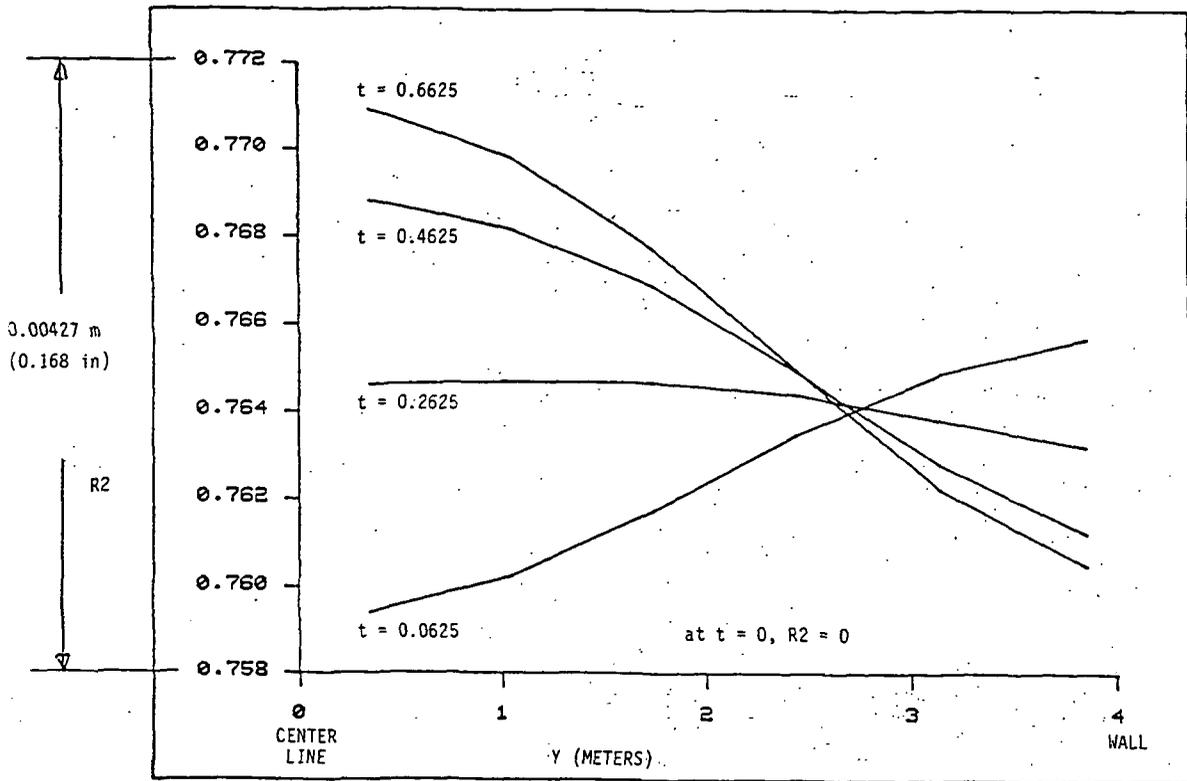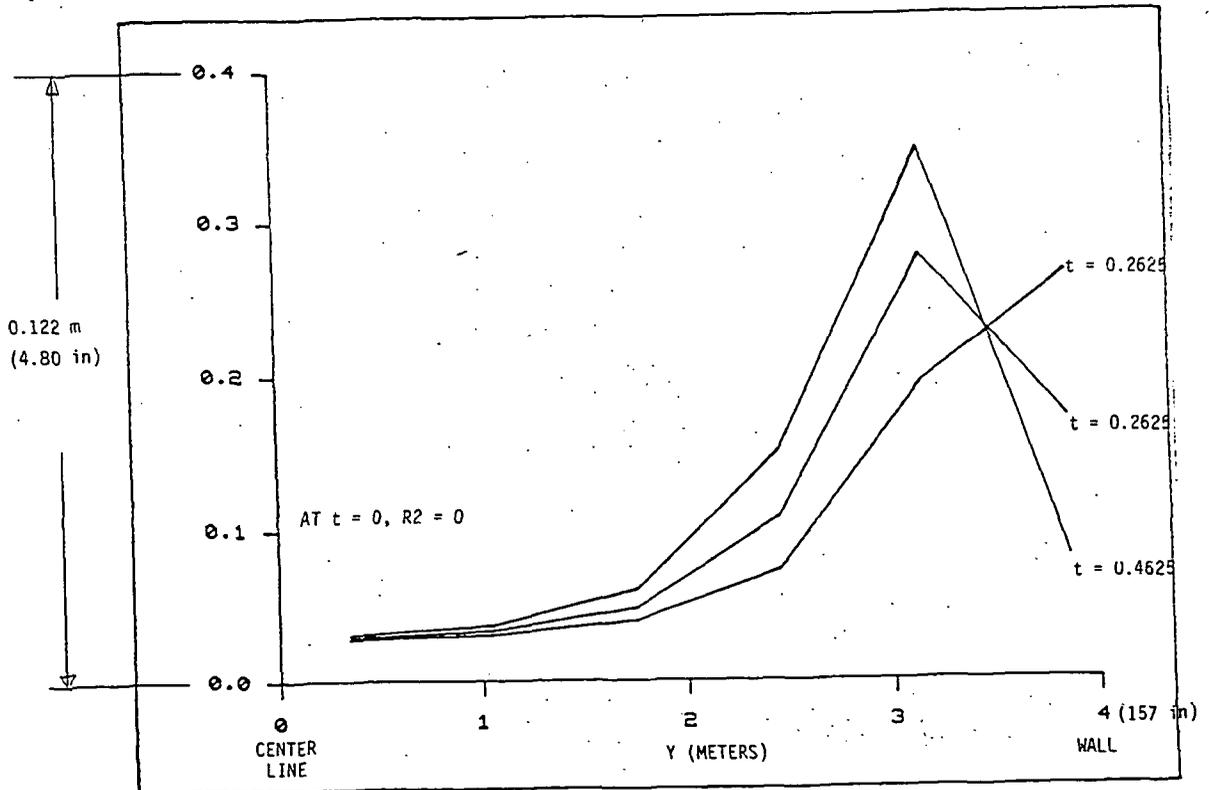
Figure B6: Case 2 Enlarged Surface Positions

B9

APPENDIX C

Interim Report on
Global Modeling of SSME

by

T. Mukerjee and A.J. Przekwas

ABSTRACT

Further refinement in the Main Injector Assembly (MIA) model has been incorporated by using realistic non-uniform velocity distribution at the two entries. Computations made for two test cases, respectively with and without shields on the outer LOX posts, show significantly increased pressure drops due to the shields and suggest correspondingly higher mechanical loads on the LOX posts. A comparison with an earlier test run made with uniform inlet velocities and shielded LOX posts reveals that the shields virtually kill the effects of non-uniformity in entry velocities and influence the velocity field in MIA strongly irrespective of the upstream conditions.

1. INTRODUCTION

As a first step in the SSME Global modeling exercise, attention has been given to the Main Inejctor Assembly (MIA). In this presentation realistic non-uniform velocity distributions at the elliptic entry at Fuel Preburner End (FPE) and at the round entry at Oxygen Preburner End (OXPE) have been provided through a "processor-program" that processes the velocity distribution in BFC system at HGM exit to the orthogonal polar coordinate system at MIA entries. Two test computations were made with and without shields on outer LOX posts respectively to study the effects of shields on pressure drop across them and the flow field. As before, in these calculations eddy viscosity was constant and density of the compressible gas is obtained from $\rho = \frac{1}{c} p^B$.

2. COMPUTATIONAL DETAILS

Figure C1 shows the grid for the calculation domain where NX=18, NY=15 and NZ=11 totalling 2970 cells. As indicated earlier (see 4045/17, Appendix D) the interface between the HGM transfer tube and the MIA is at IY=15. The fluid properties and boundary conditons are the same as before.

3. PRESENTATION AND DISCUSSION OF RESULTS

The results are presented separately for the two test cases which are:

a)   No Shields on the Outer LOX posts; and

b)   With Shields on the LOX posts.

For comparison with the latter, results of an earlier run with uniform inlet velocity at the two entries are presented only to highlight the strong influence of the shields on the flow field in MIA.

No shields on LOX Posts - Non-uniform Inlet Velocity Distribution

Figures C2 to C5 show the results obtained for this case. Figures C2 and C3 show the velocity vectors at selected XY planes and it is evident there that the flow is mainly radial with a very small amount moving circumferentially in the race track. This is also shown in Figure C4 where velocity vectors are drawn at selected YZ planes. The vectors turn downwards as the fluid finds its way out through the main injector elements. Figure C5 shows the concentration contours at selected XY planes, and the spread of the contours over the whole plane suggests that the two streams do not have a tendency to move circumferentially into each other.

The specific pressure drop across the cells containing the outer row of LOX posts. vary both circumferentially and axially; and, hence, they are indicated as a range as follows:

OXPB Side $0.11 < \Delta p_z < 39.7$ psi
FPB Side $14.3 < \Delta p_z < 126.7$ psi

The higher value of Δp_z and its wider range of the FPB side is due to 2.3 times higher mass inflow there compared with the OXPB side. A comparison with an earlier run made with uniform velocity distribution at the two entries shows that as a result of non-uniformity in velocity distribution in this case, Δp_z has gone up between 0 to 50%.

With Shields on LOX Posts - Non-uniform Inlet Velocity Distribution

Figures C6 to C9 show the predicted flow field in MIA, and they indicate strong influence of the shields (on the outer row of the LOX posts). In

Figures C6 to C7 it can be seen that a portion of the flow from FPB side moves circumferentially along the race track (also see Figure C9) to join the fluid from OXPB side and flow radially towards the center of the calculation-domain. This combined stream pushes across the center to the FPB side to produce a recirculating region there. Close to the shields, on their downstream, flow recirculations occur at both FBP and OXPB sides particularly between 0.3L and 0.8L. Such phenomena were absent in the previous case.

As a consequence of the flow non-uniformities and the presence of the shields in the flow field, the pressure drop across the cells containing the outer LOX posts with shields are higher than in the previous case (without shields). The average increase in static pressure drop there is given below.

OXPB Side   73.2 psi
FPB Side   110.3 psi

Such increases in pressure drop will obviously increase the mechanical loading of the LOX posts more on the FPB side than on the OXPB side. This is confirmed by the buckling and deformation of the LOX posts on FPB side observed in SSME after test flight/run.

An earlier test run with uniform velocity at the entries and shields on outer LOX posts showed virtually the same velocity fields as in Figures C6 to C8; and, an increase in pressure drop of almost the same magnitude as above over the case without shields and uniform entry velocity. This suggests that velocity non-uniformities at shields-upstream are outweighed by very strong influence of the shields on the flow in MIA.

4. CONCLUSIONS AND RECOMMENDATIONS

It is concluded that:

-       The computed flow fields for the calculation domain with and without
        shields on LOX posts are plausible;

-   The shields have a strong influence on the flow field in MIA and flow
    non-uniformities on shield-upstream have little effect on shield-
    downstream in MIA;

-   The shields cause a significant increase in pressure drop across
    themselves which increases the mechanical loads (on the outer LOX
    posts that carry the shields); and this could cause deformation and
    failure of LOX posts in MIA.

It is recommended that:

-   The processor-program that facilitates data input from 1D to 3D and
    vice-versa, from 2D to 3D and vice-versa should now be applied to a
    number of test cases to demonstrate its capability before applying it
    to a combined HGM-MIA analysis.
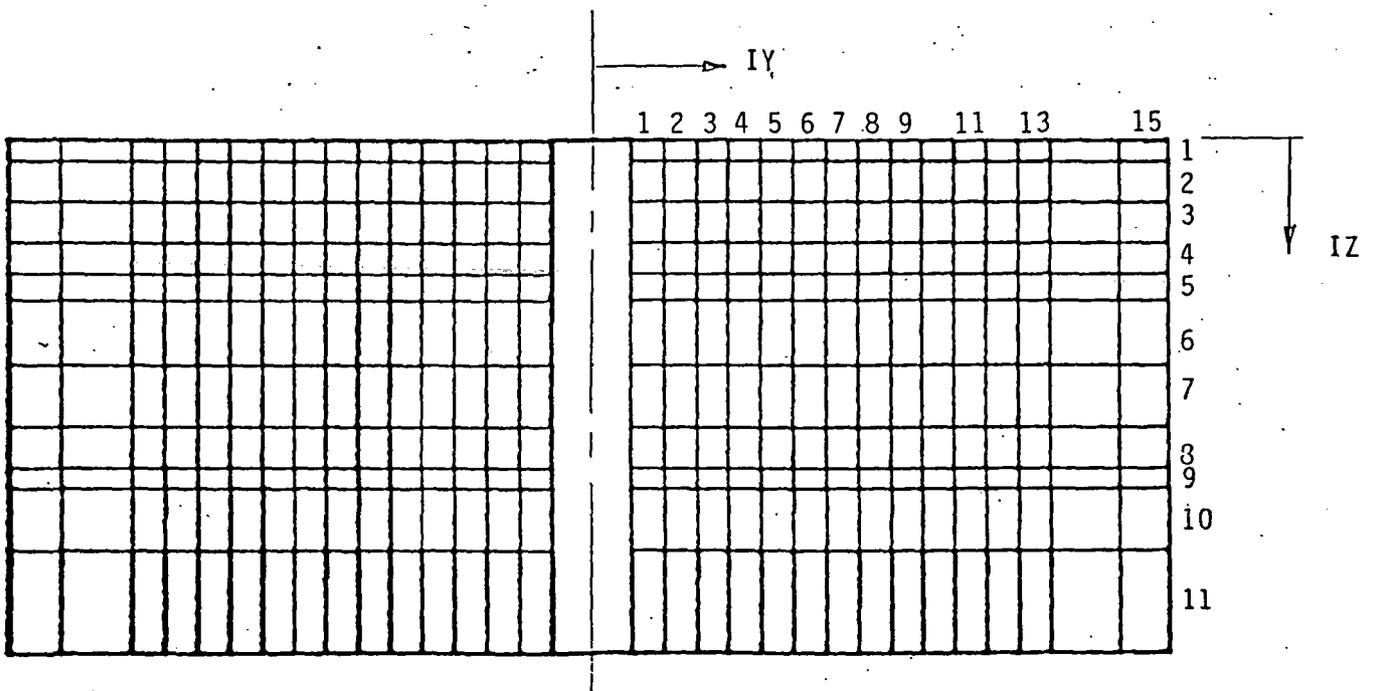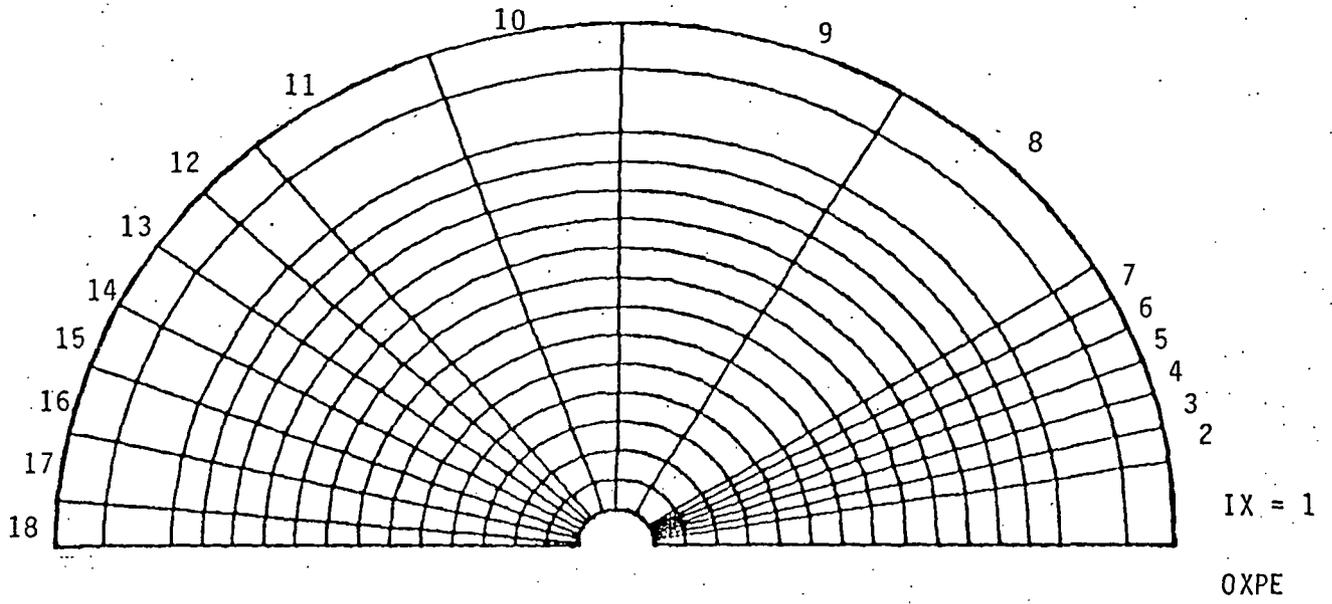
Figure 61: Grid Used in MIA, NX=18, NY=15, NZ=11   2970 Control Cells

0.1L

0.2L

0.3L

0.4L
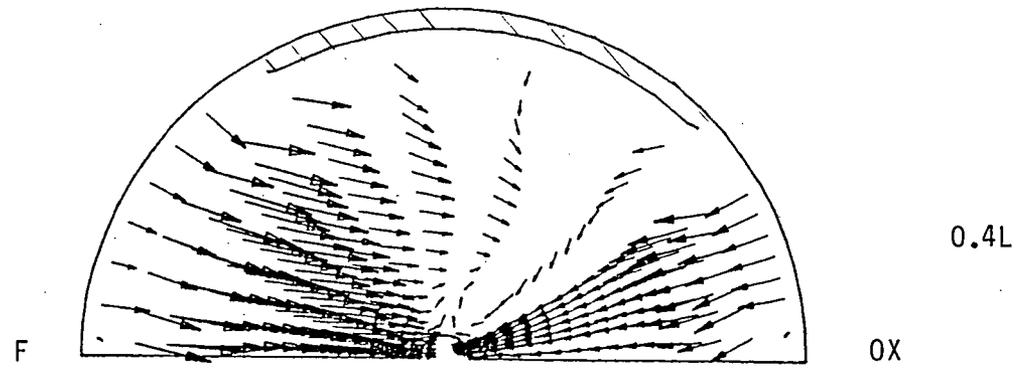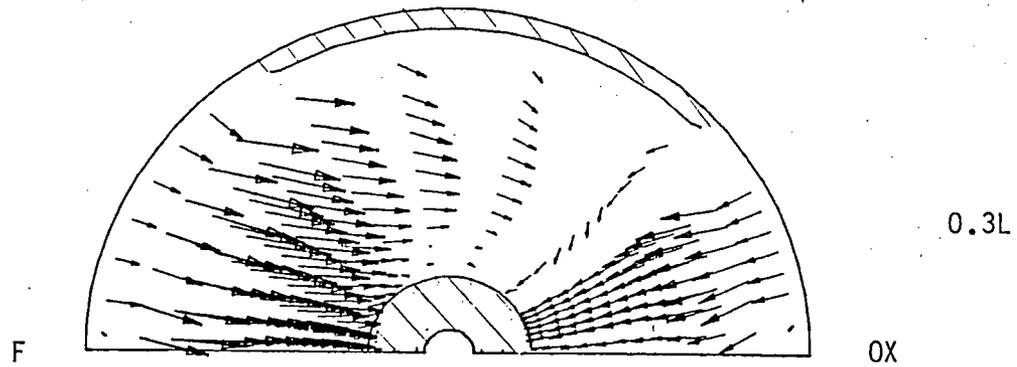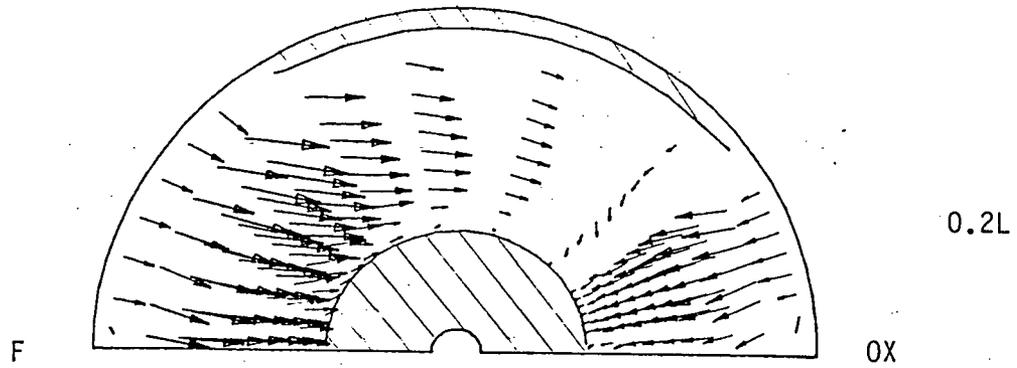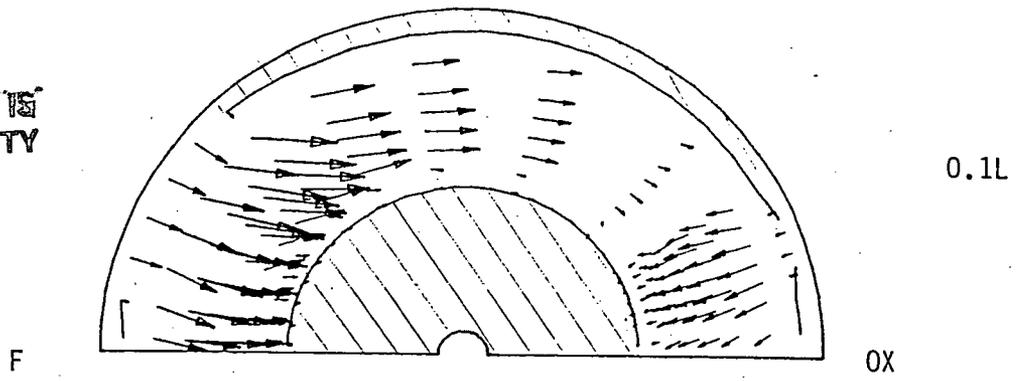
Figure C2: Velocity Vector Plot in MIA – No Shields

C6

0.5L

OX

F

0.6L

OX

F

0.7L

OX

F
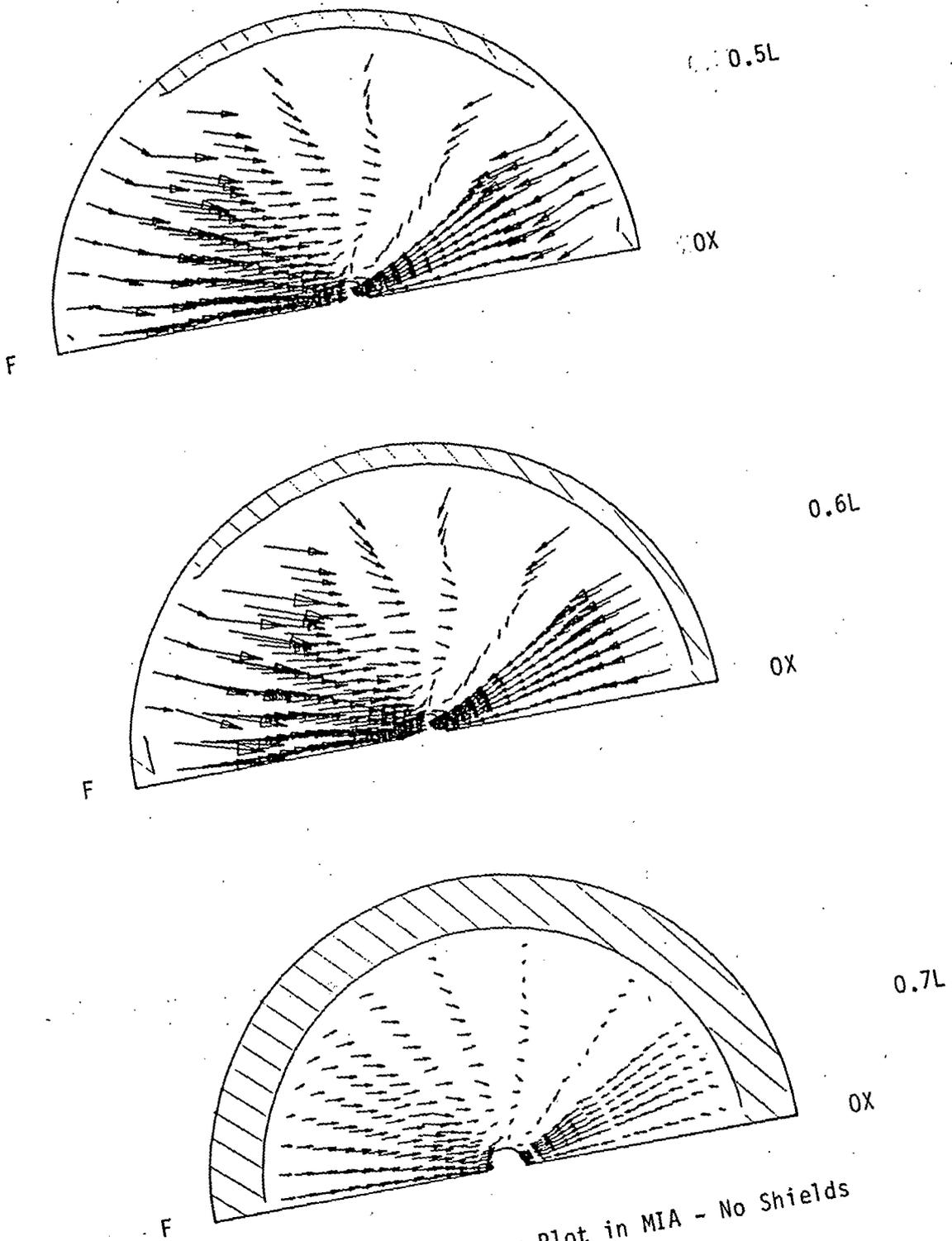
Figure C3: Velocity Vector Plot in MIA – No Shields

//// Bloc

L = Lengt
Calculat
Domain =

F = Fuel Preburner
    Side

OX = Oxygen Preburner
     Side

$\theta = 170^O$ $\theta = 10^O$

F   OX

$\theta = 160^O$ $\theta = 20^O$

F   OX

$\theta = 150^O$ $\theta = 30^O$

Figure C4: Velocity Vector Plot in MIA - No Shields

0.2L

0.4L

0.6L
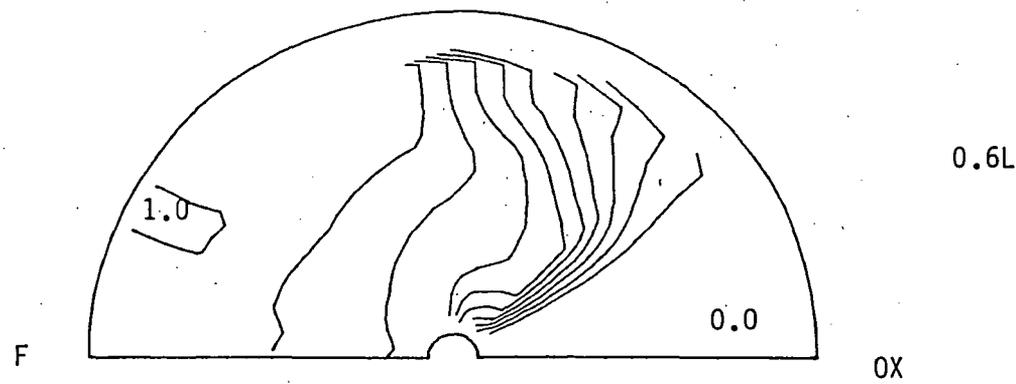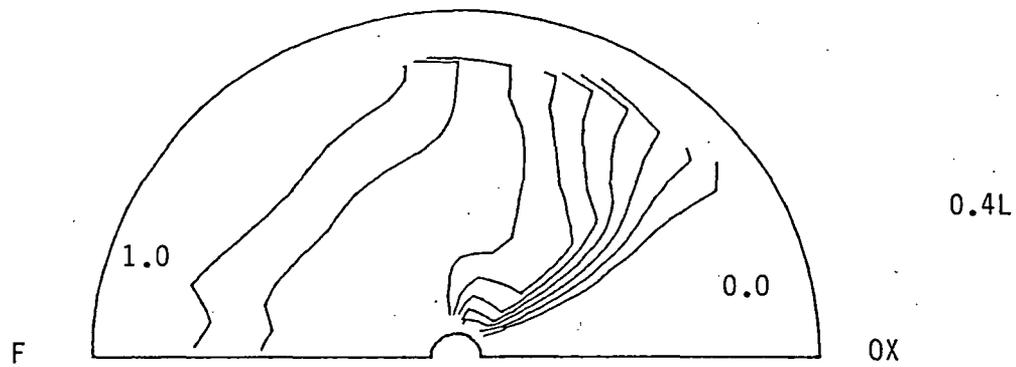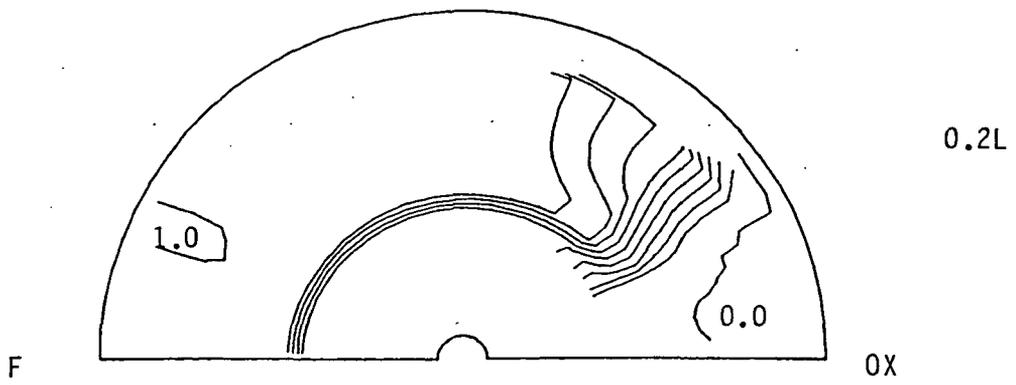
Figure C5:   Concentration Contour Plots in MIA - No Shields
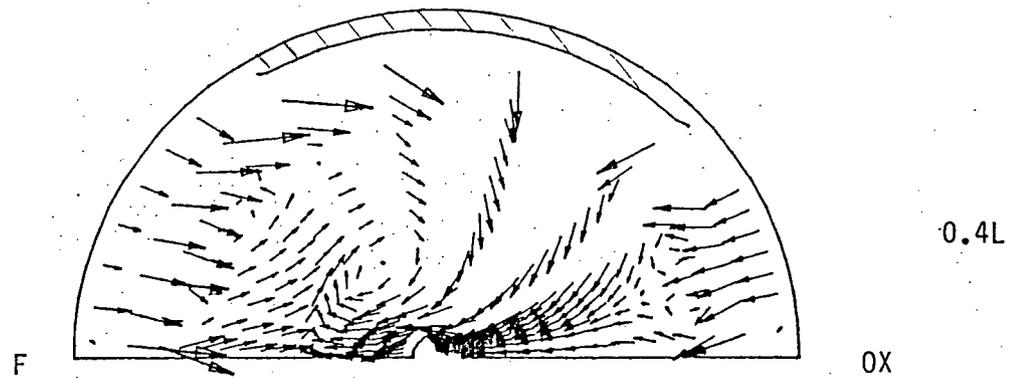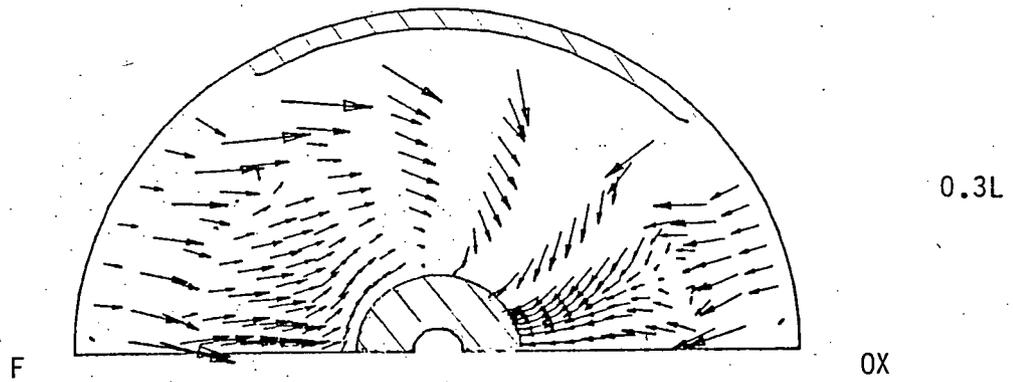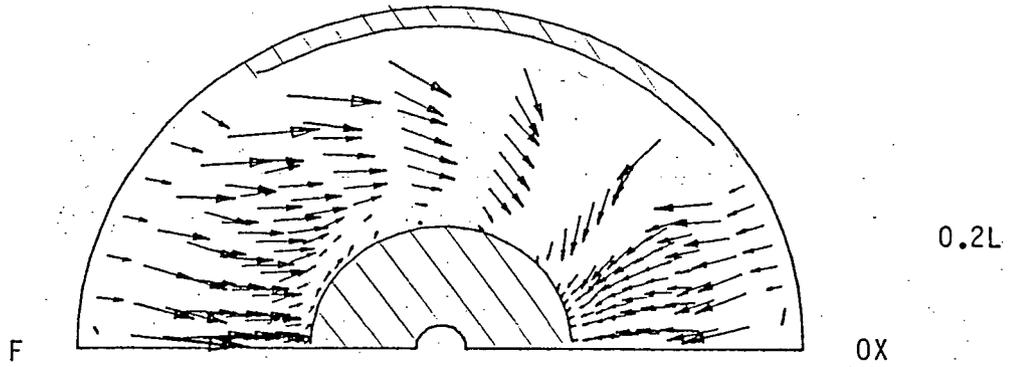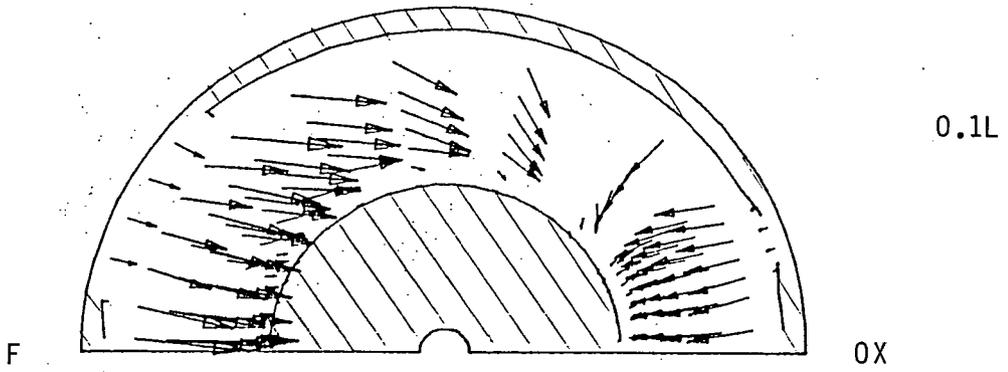
Figure C6: Velocity Vector Plot in MIA - With Shields

/// Blocked

0.1L

0.2L

0.3L

0.4L

F

OX

0.5L

F

OX

0.6L

F

OX

0.7L

F

OX
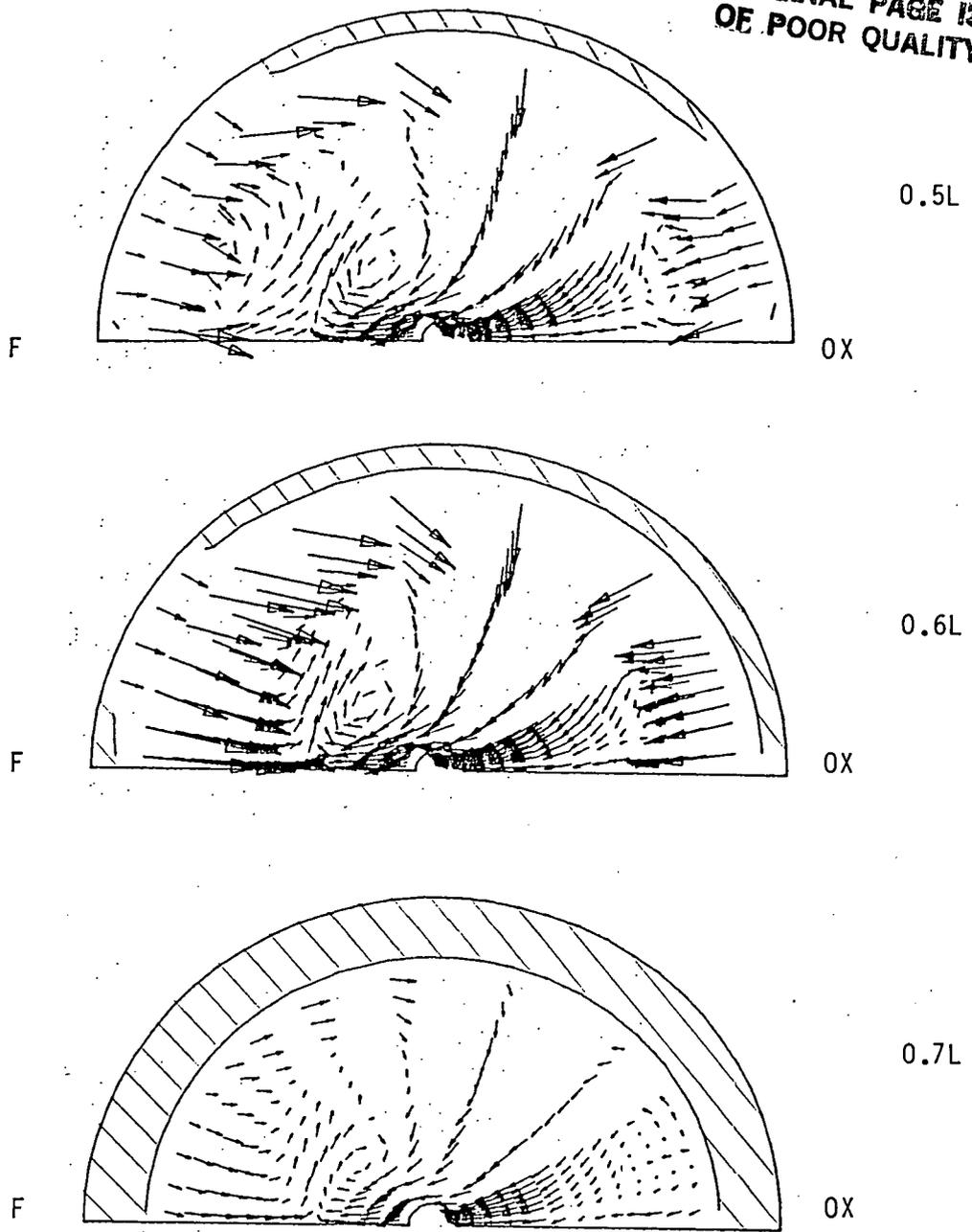
Figure C7: Velocity Vector Plot in MIA - With Shields

F = Fuel Preburner Side

OX = Oxygen Preburner Side

/// Blocked

L = Length of
Calculation
Domain
= 10"

$\theta = 170^{0}$ $\theta = 10^{0}$

F   OX

$\theta = 160^{0}$ $\theta = 20^{0}$

F   OX

$\theta = 150^{0}$ $\theta = 30^{0}$

F   OX
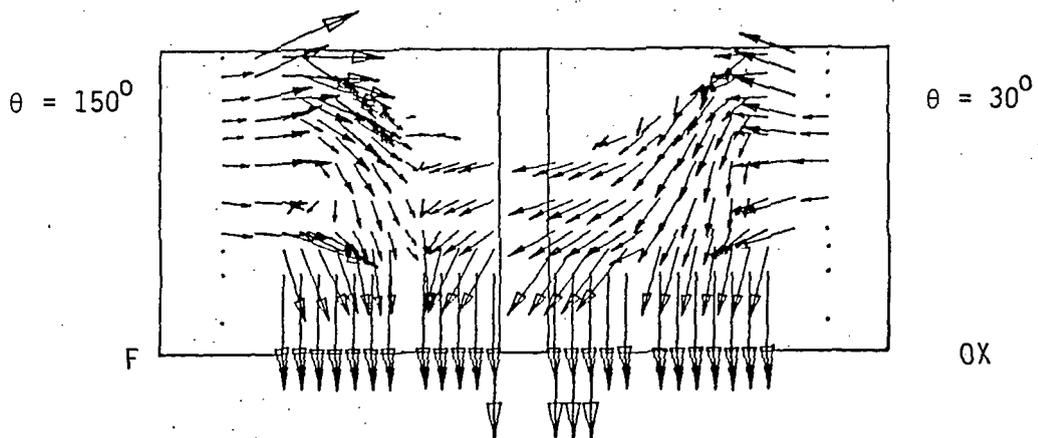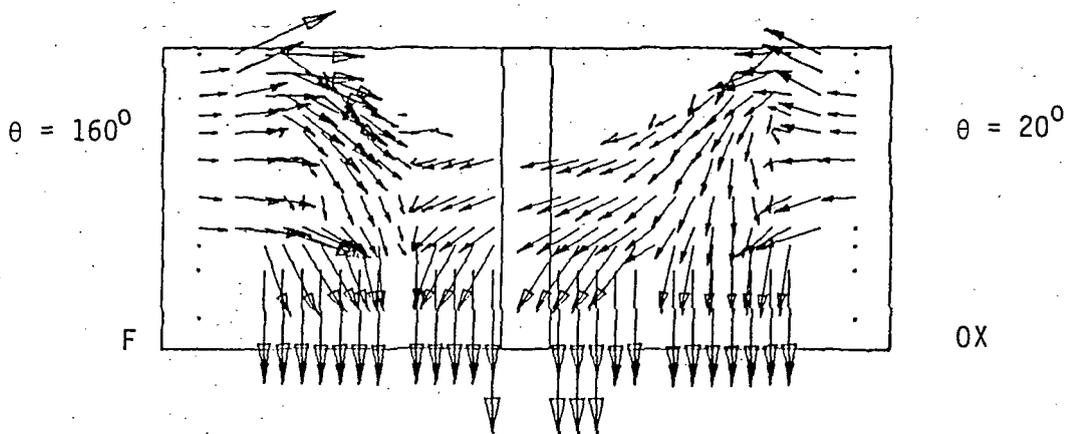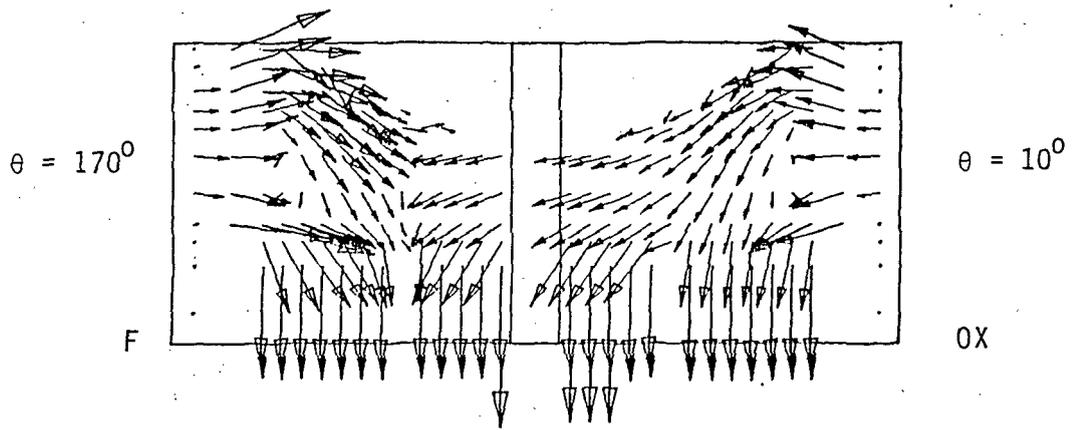
Figure C8: Velocity Vector Plot in MIA - With Shields
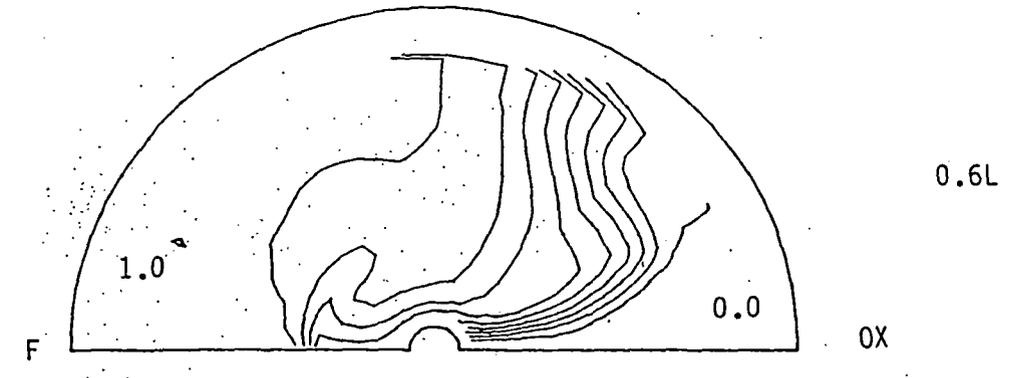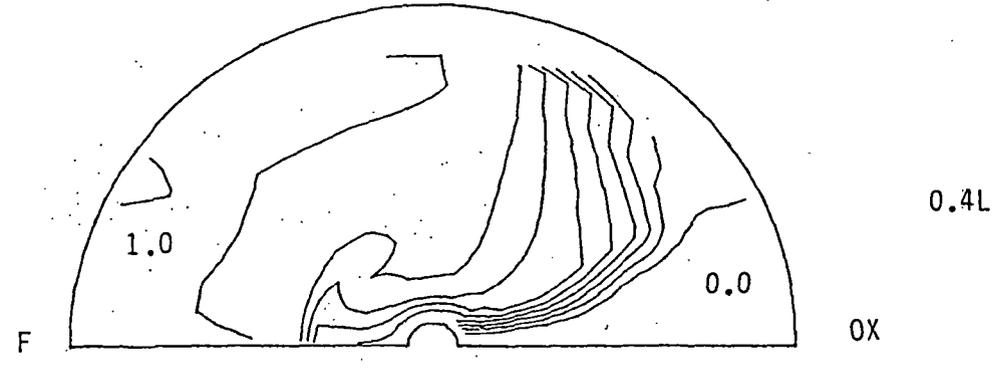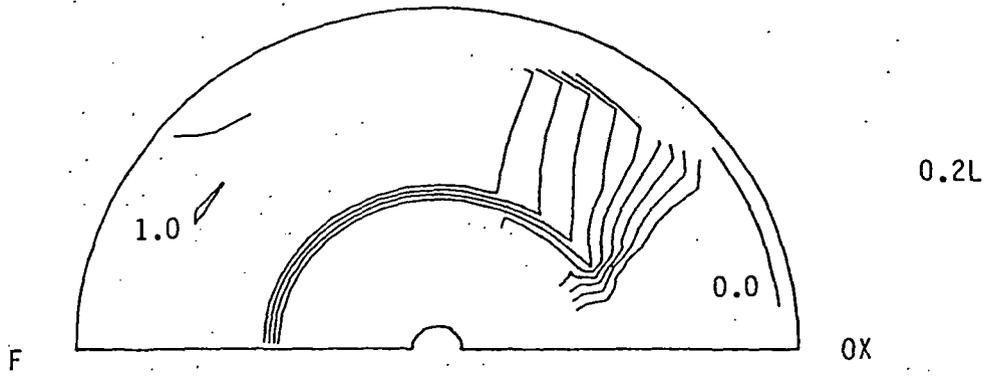
Figure C9: Concentration Contour Plots in MIA - With Shields

APPENDIX D

INTERIM REPORT ON SIMULATION OF LOX MOTION
IN SHUTTLE EXTERNAL TANK DUE TO WALL STRUCTURAL DEFORMATIONS

By

A.K. Singhal, A.J. Przekwas and M. Kannapel

APPENDIX D

INTERIM REPORT ON SIMULATION OF THE LOX MOTION
IN SHUTTLE EXTERNAL TANK DUE TO WALL STRUCTURAL DEFORMATIONS

ABSTRACT

Since last month many important steps have been accomplished: the donor-acceptor technique in PHOENICS has been tested to ensure grid-independent solutions; all surface deflections are following a sinusoidal curve instead of a ramp function; the External Tank geometry has been entered into the model by using a porosity concept; and the entire surface of the external tank is being moved at a four H_2 frequency but with a different deflection amplitude and direction at every cell. The anticipated next steps are outlined.

1. INTRODUCTION

Last month's report included results from a cylindrical tank problem with only one cell being deflected at various locations by a ramp deflection curve. This month, the grid for the actual external tank has been formulated (see Figure 1) with the LOX motion being induced by deflecting the entire tank wall with a sinusoidal curve of different amplitudes and directions at every cell. These amplitudes and directions were determined from the data supplied by NASA. Additionally, tests were done to ensure that the donor-acceptor technique is grid independent. Work on Task 1 (check-out calculations) has been completed and work on Task 2 (Analysis of the LOX Surface Motion in External Tank) is in progress.

2. COMPUTATIONAL DETAILS

Task 1 - The cylindrical tank with wall deflection at the bottom has been selected for the grid dependence studies; two grid systems 29 and 19 grids in the axial direction. Flow conditions are exactly the same as those reported in our previous progress report. The grid refinement has been accomplished by doubling the number of grids (in the surface motion zone) in comparison with the coarse grid case. One cycle of the oscillations has been simulated.

Task 2 - The grid used in the real tank case consists of 12 cells in the radial direction and 31 cells in the axial direction with the closest spacing being near the LOX surface (see Figure 1). The shape of the tank wall was formed by using the porosity concept.

The deflection of the single cell (in the grid-dependence case) and of each of the wall cells in the real tank case were achieved by changing the porosity at each cell (for each time step) in accordance with a sinusoidal wave. Like previous test problems, the time step was 0.00625 sec which was obtained by dividing each cycle into four quarter cycles of ten time steps each.

3. PRESENTATION AND DISCUSSION OF RESULTS

Task 1 - In the grid dependence case the wall was displaced near the bottom of the tank at one location using a sinusoidal time deflection curve. Figures 2 and 3 show velocity vectors and magnified surface locations at t = .125 sec. (half cycle) and t = .25 sec (full cycle) for both coarse and refined grid test cases.

These results show that a sinusoidal deflection curve (as opposed to a ramp curve) can be used to yield good results throughout the cycle. The velocity vectors in both the fine and coarse grid are basically uniform in the radial direction which causes the surface to remain almost flat throughout the deflection cycle. The surface location and velocities are nearly identical for both grids verifying that the donor-acceptor technique is grid independent. This case closes out Task 1 of the four proposed tasks.

Task 2 - Velocity vectors and surface location for the real tank at two different time steps are provided in Figure 4. The model seems to respond to imposed deflection curves in a reasonable manner. The surfaces rises much more at the wall than at the center. The velocity vectors, shown in Figures 4a and 4b, indicate that the surface motion and shape are the most sensitive to the wall deflections in the direct neighborhood of the liquid surface level. The velocity vectors within the bulk of the liquid volume remain almost uniform.

4. CONCLUSIONS AND RECOMMENDATIONS

Several important steps have been accomplished this month: sinusoidal deflection curve, grid-dependence study, insertion of tank shape, and accurate deflections at each cell. Task 1 has been completed and all remaining calculations will be focused on the real tank geometry. The next step is to run the current model for a few cycles to determine if it is providing accurate predictions. Additional printout of auxiliary variables will be provided including total tank volume variation, surface accelerations, etc. Results from the basic test case are currently being analyzed and will be discussed in detail in our next report. Two test cases will be compared with

four and seven baffles inserted into the flowfield. Then two different LOX heights will be examined for the four baffle case.
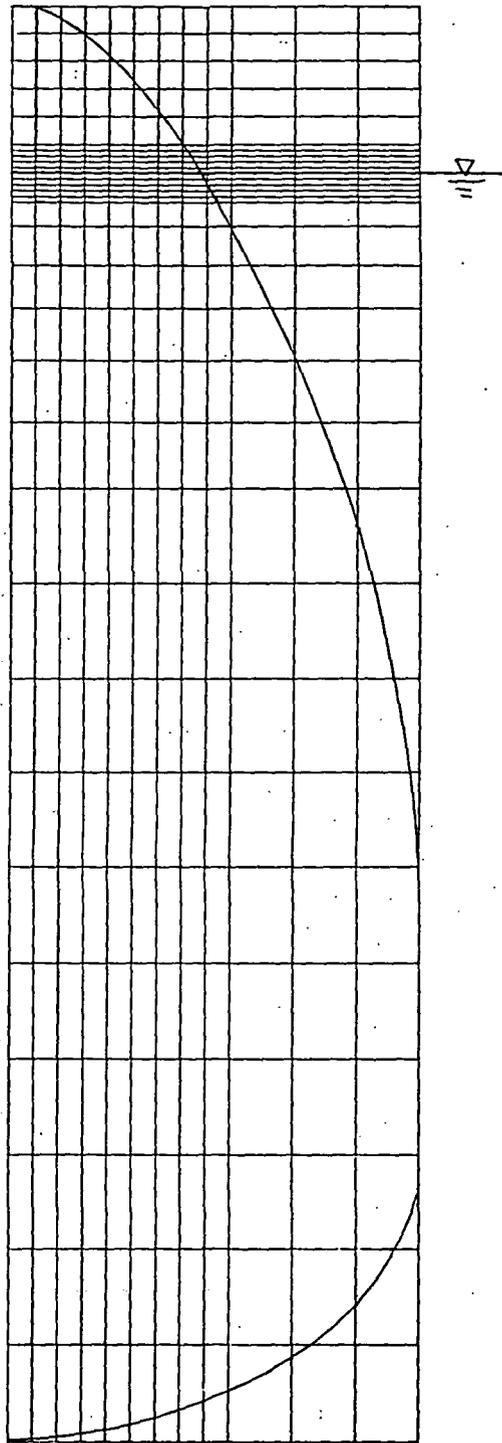
Figure 1

Computational Grid

FINE GRID (t = 0.125 sec)

COARSE GRID (t = 0.125 sec)

FINE GRID (t = 0.25 sec)

COARSE GRID (t = 0.25 sec)
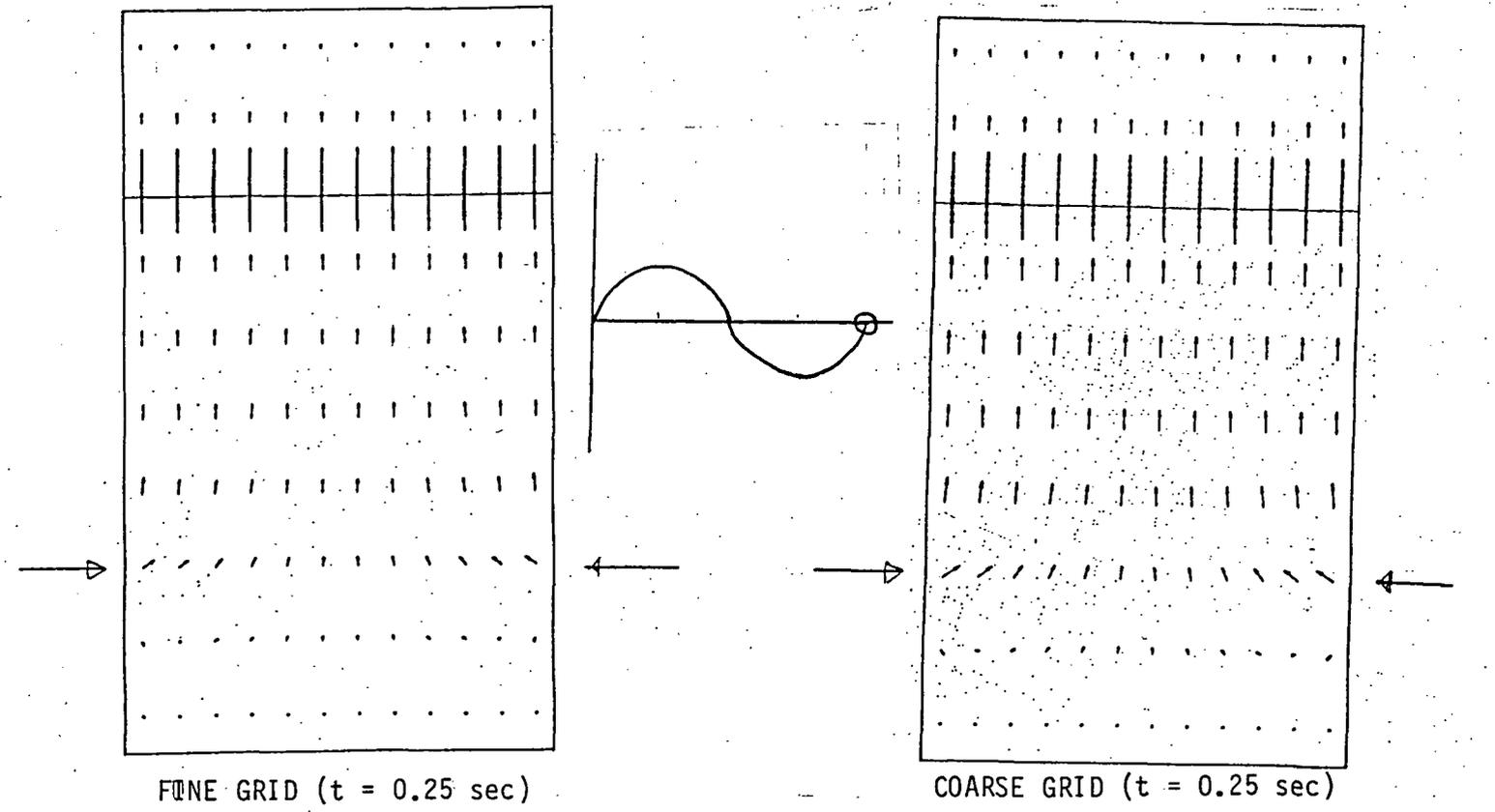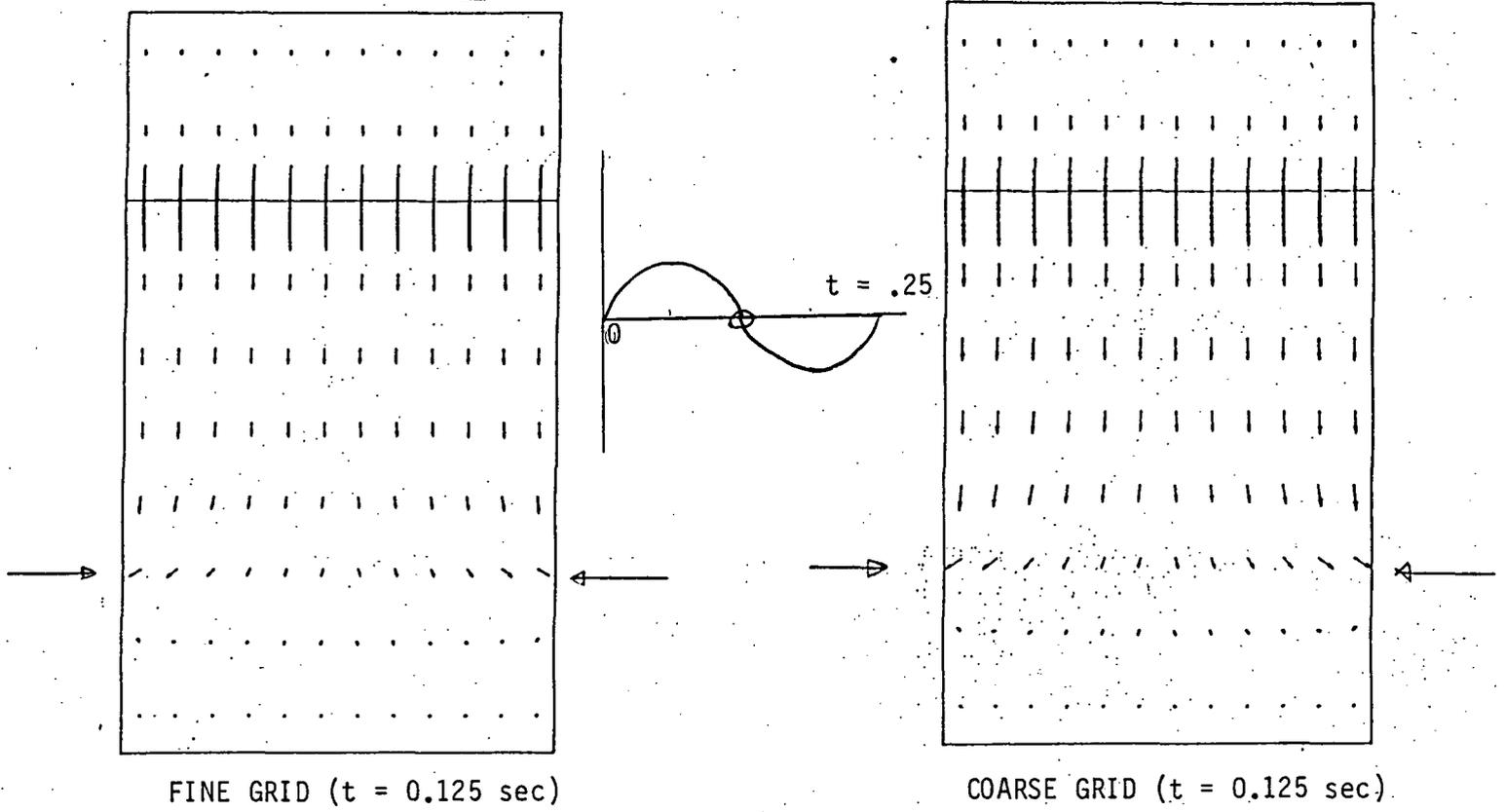
FIGURE 2

MAGNIFIED SURFACE LOCATIONS

COARSE GRID (t = 0.125 sec)

FINE GRID (t = 0.125 sec)
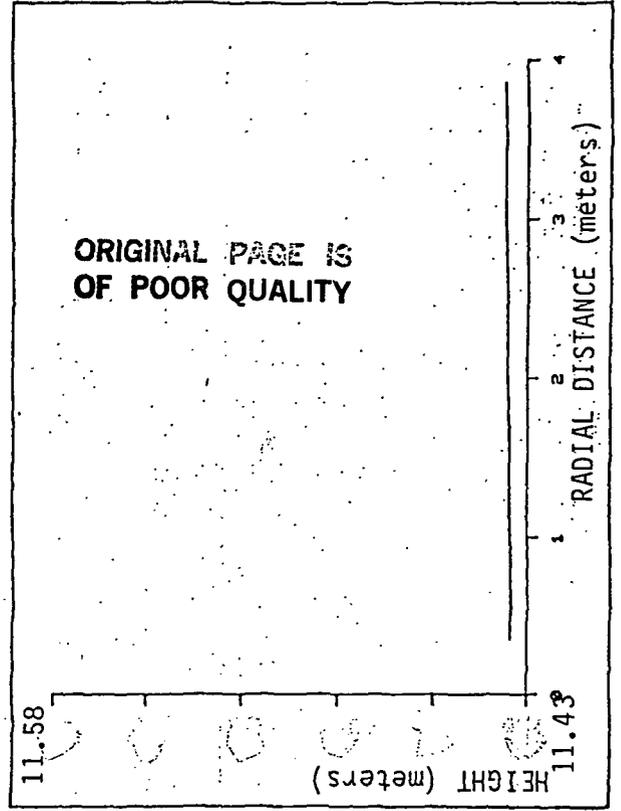
COARSE GRID (t = 0.25 sec)

FINE GRID (t = 0.25 sec)

Figure 3
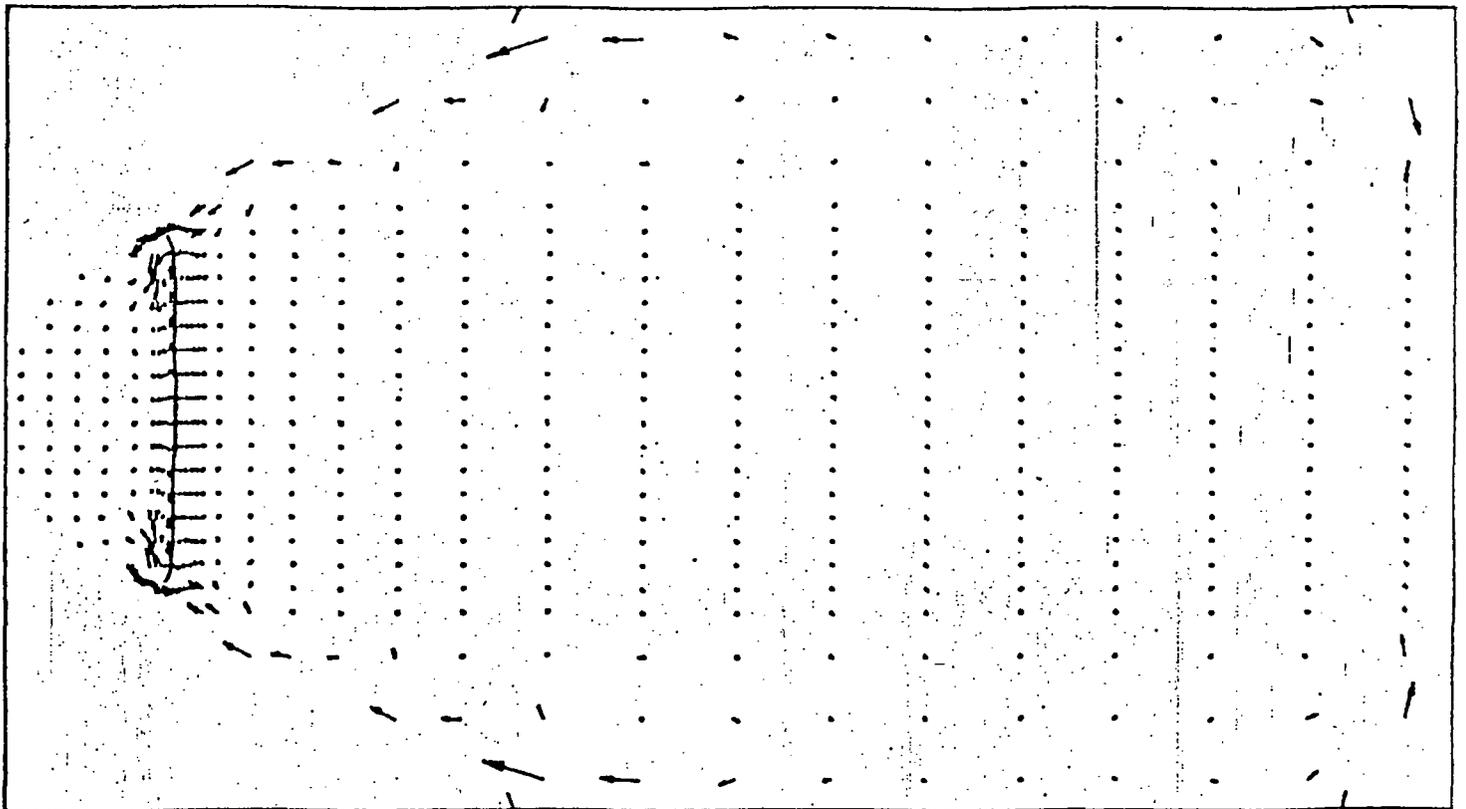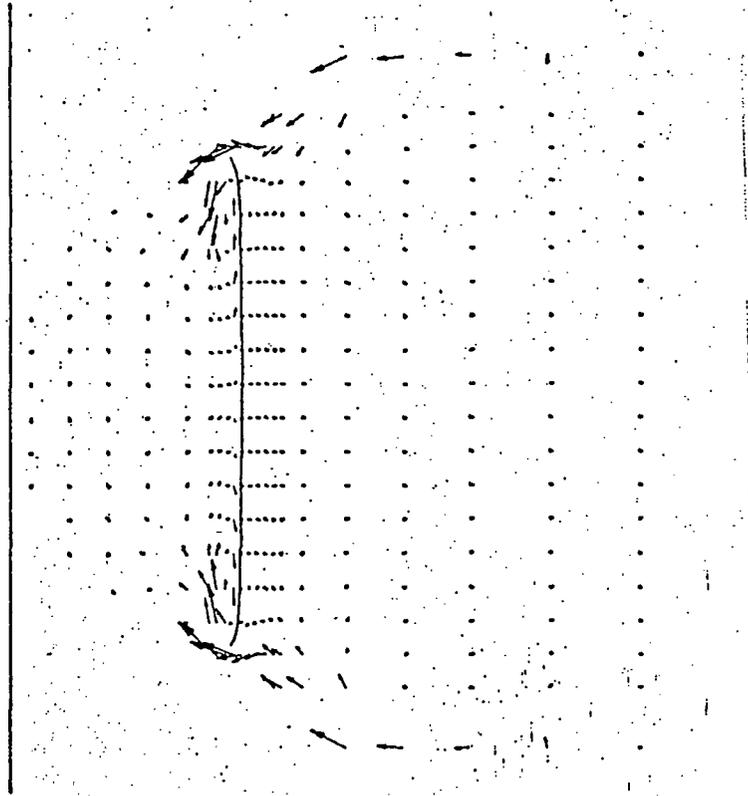
Figure 4a
Velocity Vectors of External Tank at t = .0625 sec

Figure 4b

CHAM